HOKKAIDO UNIVERSITY

Title	Typhoon disturbance effect on forest dynamics and carbon balance at a cool-temperate forest in northern Japan simulated by SEIB-DGVM
Author(s)	烏, 蘭
Degree Grantor	北海道大学
Degree Name	博士(農学)
Dissertation Number	甲第13917号
Issue Date	2020-03-25
DOI	https://doi.org/10.14943/doctoral.k13917
Doc URL	https://hdl.handle.net/2115/77844
Type	doctoral thesis
File Information	Wu_lan.pdf



Hokkaido University Collection of Scholarly and Academic Papers : HUSCAP

Typhoon disturbance effect on forest dynamics and carbon balance at a cool-temperate forest in northern Japan simulated by SEIB-DGVM

(SEIB-DGVMを用いた北日本の冷温帯林における森林動態と炭素収支に対する台風撹乱の影響の解明)

北海道大学　大学院農学院

共生基盤学専攻　博士後期課程

烏　蘭

Contents

Abstract 1

I. Introduction 4

II-1. Background 5

II-1-1. Impact of typhoon disturbance on forest ecosystem 5

II-1-2. Dynamic global vegetation models 7

II-2. Purpose of this study 8

II-3. Composition of this thesis 9

II. Methods 10

II-1. Site description 11

II-2. SEIB-DGVM 14

II-2-1. Overview 14

II-2-2. Carbon cycle 15

II-2-3. PAR 18

II-2-4. Photosynthesis 19

II-3. Model setting 20

II-3-1. Leaf phenology for Japanese larch 23

II-3-2. Establishment 23

II-3-3. Mortality 24

II-3-4. Scenario experiment design in the future 26

II-4. Climate data 29

II-4-1. Input data of SEIB-DGVM 29

II-4-2. Climate data sources at different simulation periods 29

II-4-3. Validation data 31

III. Results 33

III-1. Model validation 34

III-2. Variations of carbon and forest dynamics in the past 38

III-3. Effect of typhoons on forest structure in the future 40

III-3. Effect of typhoons on carbon dynamics 49

IV. Discussion 59

IV-1. Representativeness of forest and carbon dynamics in the past and present after two typhoons 60

IV-2. Effect of typhoon disturbance on forest dynamics in the future 63

IV-3. Effect of typhoon disturbance on carbon dynamics in the future 69

IV-4. Limitations 74

V. Summary 75

VI. References 78

VII. Acknowledgments 89

VIII. Appendix 92

IX. Abbreviations 99

Abstract

Large storm is a major source of natural disturbance in forest ecosystems in coastal regions of the world. Under the changing climate, some climate projection models predict that storms would become stronger in future, especially in Northwest Pacific region. Although the destruction of typhoons has a strong impact on the structure and carbon balance of forest ecosystems, leading to local climate change feedback, the long-term effect of typhoon frequency and intensity on forest and carbon dynamics has not been investigated especially from the perspective of future climate change. To elucidate these long-term effects, a SEIB-DGVM (Spatially explicit individual-based dynamic global vegetation model) was applied to a deciduous-coniferous mixed forest in southern Hokkaido, Japan, to represent the development of a larch plantation established in 1954 after typhoon Toyamaru struck a natural forest and the natural regeneration from 2004 when the plantation suffered windthrow by typhoon Songda. The model was validated to ground measurement of eddy flux and biomass. The adapted model was then forced with various combinations of typhoon scenarios with multiple frequency and intensity levels, and with the projected climatic conditions for 2017–2100 under Representative Concentration Pathways (RCPs) 2.6 and 8.5. The aims of this study are: (1) reproducing the forest structural traits and carbon dynamics in Tomakomai in the historical period by using SEIB-DGVM; and (2) evaluating the possible impact of typhoons on the forest under projected future climate changes.

The validation result shows that SEIB-DGVM could reproduce the interannual variations at the Tomakomai Flux Research Site in historical period. The future projections suggest that increasing typhoon frequency and intensity have a significant effect on forest and carbon dynamics under both RCP 2.6 and RCP 8.5. As the frequency

and intensity of typhoons increase, aboveground biomass (AGB) and net primary production (NPP) decrease. However, increasing typhoon frequency and intensity had a greater influence on AGB than NPP. The values of AGB and NPP are much higher under RCP 8.5 than under RCP 2.6 and at baseline. As the frequency and intensity of typhoons increase, net ecosystem production first increases and then decreases. The projection indicates that the forest at the Tomakomai site will become a carbon sink under different typhoon scenarios at the end of the 21st century. The result also predicts that if typhoon frequency is $\leq$ 2 (i.e., a typhoon occurs up to two times between 2017 and 2100) and intensity is $\leq$ 40% (i.e., up to 40% of trees damaged), then forest AGB can recover to that before typhoon Songda by the end of the 21st century. Simulation results also showed strong linear relationships among forest structural traits (AGB, tree height, tree density, and woody plant and grass leaf area indexes), carbon fluxes, and typhoon frequency and intensity.

I. Introduction

II-1. Background

II-1-1. Impact of typhoon disturbance on forest ecosystem

Large storm is one of major natural disturbances that give the significant impacts on terrestrial ecosystems in coastal regions of the world (Chambers et al., 2007, Lindroth et al., 2009, Usbeck et al., 2010). In North America, Negrón-Juárez et al. (2010) estimated that 161.7 ± 30.9 million and 115.4 ± 24.7 million trees were destroyed by hurricanes Katrina (equivalent to a biomass loss of 43.9 ± 8.4 Tg C) and Rita (equivalent to 37.9 ± 6.4 Tg C), respectively, in 2005. Schelhaas et al. (2003) estimated that annual average storm damage in Europe was 18.6 million m^3 of wood from 1950 to 2000. In East Asia, typhoons also frequently hit forest ecosystems. In Japan, typhoons Toyamaru in 1954 and Songda in 2004 caused wind thrown tree losses over areas of 7,500 and 370 km^2, respectively (Yamanoi et al., 2015).

Large storm disturbance can play an important role in forest dynamics in temperate regions. Forest structural traits, such as species composition, tree height, tree size, and stand density, are under strong control of wind disturbance (Lin et al., 2011, Yoshida et al., 2011, Tanner et al., 2014, Chi et al., 2015, S. Chen et al., 2017, Sato et al., 2017). Foster (1988) examined species and stand responses to catastrophically strong winds in central New England and found that such forests showed greater damage in old forests and less damage in dense forests. Chapman et al. (2008) focused on the impacts of hurricane Katrina on forest biomass. The biomass production of investigation targeted forest was at a rate of 3.5 Mg ha^{-1} y^{-1} before the storm disturbance but reduced by 77.6 Mg ha^{-1} due to the disturbance. Chen et al. (2017) used ORCHIDEE-CAN to simulate the storm damage in forests of southern Sweden and southwestern France, and the results

indicate that this model is able to reproduce the dynamics of forest structure due to storm disturbance at a regional scale. Valinger et al. (2006) analyzed the damage due to storm Gudrun in Sweden in 2005. They showed that the greatest damage occurred in the oldest age class of forest stands. Previous studies mostly focused on the forest damage caused by large storms that had already occurred (Peltola et al., 1999, Gardiner et al., 2000, Ancelin et al., 2004), whereas others performed tree-pulling experiments or designed experiments to simulate hurricane blowdown to study the impact of hurricanes on the forest (Cooper-Ellis et al., 1999, Peltola et al., 2000). However, few studies have investigated the potential forest damage due to large storms under future changing climatic conditions.

Typhoon represents a major disturbance scheme for temperate forests in Asian monsoon areas (Wang et al., 2004, Xu et al., 2004, Hirata et al., 2007, 2014, Sano et al., 2010, Yamanoi et al., 2015). As wind disturbance converts living biomass into the litter pool, the forests' carbon sequestration capacity also decreases. Yamanoi et al. (2009) reported that the annual net ecosystem production (NEP) became negative after typhoon Songda, meaning that the forest changed from a carbon sink to a source. Chen et al. (2014) examined the short-term effect of frequent strong typhoons on defoliation and net ecosystem exchange (NEE) in a subtropical mangrove forest. The results showed that daily NEE responses are highly variable following different typhoons, due to the balance between the changes of gross ecosystem production and ecosystem respiration (RE). Sano et al. (2010) investigated the effect of typhoon disturbance on the carbon balance of the larch forest at the Tomakomai Flux Research Site and showed that the ecosystem shifted from a carbon sink to a source after the typhoon.

Under climatic projection conditions, tropical cyclones are expected to be more intense (2% to 11% increase) and less frequent (by −6% to −34%) by the year 2100 (Knutson et al., 2010, Chan et al., 2015). In fact, the current warming trend has already seriously affected tropical cyclone activity (Webster et al., 2005, Field et al., 2012, Mei et al., 2015, Mei and Xie, 2016). Therefore, it is important to investigate the potential response of forests to various typhoon scenarios with multiple frequency and intensity steps to understand the potential effect of disturbance on forest ecosystems.

II-1-2. Dynamic global vegetation models

Dynamic global vegetation models (DGVMs) have been developed by integrating biogeography, biogeochemistry, biophysics, and vegetation dynamics models (Cramer et al., 2001, Sitch et al., 2008, Fisher et al., 2018). DGVMs are forced by time series of climatic conditions and simulate the spatio-temporal changes in vegetation cover based on physiological capacity of multiple plant functional types (PFTs) and as well as material cycles, such as carbon and water pools and fluxes. Among these models, SEIB-DGVM (Spatial Explicit Individual-Based Dynamic Global Vegetation Model; Sato et al., 2007) is characterized by its representation of plant population dynamics: individual trees grow in a spatially explicit virtual forest, where trees compete for light and space (Sato et al., 2010). This way of reproducing the forest structure allows SEIB-DGVM to assess the effect of typhoons on plant population dynamics and the carbon balance by explicitly representing the typhoon damage to individual trees.

SEIB-DGVM has been implemented on a plot (Sato et al., 2010), regional (Sato and Ise 2012), and global scale simulations (Sato et al., 2007). SEIB-DGVM was well validated in a simulation of forest structure and function in a larch forest in eastern Siberia

(Sato et al., 2010). Ichii et al. (2010) used the data from four eddy flux observations sites in Japan to calibrate nine terrestrial biosphere models. After the calibration, most models including SEIB-DGVM were able to represent the seasonal and interannual variations in the carbon cycle. Therefore, SEIB-DGVM is considered to be appropriate for simulating cool-temperate forest dynamics. In the simulation of forest disturbance, SEIB-DGVM was mainly used in wildfire studies (Sato et al., 2007, 2010), whereas few studies focused on typhoon disturbance. Fujii et al. (2009) introduced sprouting regeneration and typhoon disturbance into SEIB-DGVM to investigate the resilience of stand structure and tree species diversity. In simulations of stand development and succession, this model reproduced the regeneration dynamics from young secondary to old-growth stands well.

II-2. Purpose of this study

In this study, SEIB-DGVM was applied to simulate the effect of typhoons on plant population dynamics and the carbon balance in a cool-temperate forest. To evaluate the potential response of forest ecosystems under typhoon disturbances over a range of frequencies and intensities, SEIB-DGVM was applied first to historical events of typhoon disturbance and the subsequent establishment of an artificial larch plantation and natural mixed forest recovery at the Tomakomai Flux Research Site during 1901–2016. Then a future simulation was conducted from 2017 to 2100 with varying combinations of typhoon intensity, typhoon frequency, and climate scenarios. The aims of this study are: (1) reproducing the forest structural traits and carbon dynamics in Tomakomai in the historical period by using SEIB-DGVM; and (2) evaluating the possible impact of typhoons on the forest under projected future climate changes.

II-3. Composition of this thesis

Chapter 1 introduces the background of typhoon disturbance effect and dynamic global vegetation models. And the purpose of this study is to reconstruct the forest and carbon in historical and predict future.

Chapter 2 is about the material and methods. This chapter contains site description, overview of SEIB-DGVM and climate data. To know how the different typhoon frequency and intensity impact the forest dynamic and carbon balance, a simulation experiment for the future period was designed. Some detail information was listed in this chapter.

Chapter 3 reports the validation result of SEIB-DGVM through comparing the observation and simulation result in the history period. This part also predicts the AGB, woody LAI, grass LAI, tree height, NPP, NEP, HR in the end of 21 century under the different typhoon scenarios under different climate scenarios.

Chapter 4 discusses whether SEIB-DGVM can reconstruct the historical period in a cool temperate forest, and also compares with other studies to explain how reasonable this simulation is or not. Finally, the limitation and future potential of this study are listed.

Chapter 5 summarizes the main job which were already done in this study, and clarifies the meaningfulness of this study, and finally makes sure if this study achieves the objectives which was listed in the introduction part.

II. Methods

II-1. Site description

The study was conducted at the Tomakomai Flux Research (TMK) Site in the Tomakomai National Forest in southern Hokkaido, Japan (42.73°N, 141.52°E, 125 m a.s.l.). This site is located in the southern part of Hokkaido and 14 km away from the Pacific coastline (Fig. 1), on a flat plain with a slope inclination of less than 2°. It belongs to the cool temperate climatic zone. According to data from the Automated Meteorological Data Acquisition System (AMeDAS), the annual average air temperature in Tomakomai from 2005 to 2017 was 8 ℃ and the annual average precipitation was 1279 mm. This site is 10km from a volcano, Mt. Tarumae. The soil was developed from volcanic ash deposited from Mt. Tarumae's large eruption in 1667. The topsoil layer has good drainage but is very shallow. The soil in Tomakomai has a thin humic A horizon (<10 cm) and thick C horizons derived from pumice deposited by the eruptions of Mt. Tarumae in 1667 and 1739. The organic layer is about 3 cm thick (Sakai, 2007).

After the catastrophic destruction of the forest due to typhoon no. 15 (Toyamaru) in 1954, Japanese larch *(Larix kaempferi*) was planted during 1957–1959. By 2004, it had grown to be a middle-aged forest mainly composed of Japanese larch, birch (*Betula ermanii, Betula platyphylla*), and fern (*Dryopteris crassirhizoma, Dryopteris austriaca*) (Fig. 2; Hirata et al., 2014). Typhoon Songda hit the site in 2004, and 90% of the trees were blown down, most of which were uprooted. The trunks of fallen trees were removed for timber, whereas branches, leaves, and coarse woody debris were left in place (Fig. 3; Hirano et al., 2017). By 2010, saplings of deciduous trees became conspicuous. In 2014, birch dominated as pioneer species and accounted for 51% of the population and 78% of the biomass of the forest (Fig. 4). Other major woody species in the forest are *Magnolia*

kobus, Maackia amurensis, L. kaempferi, Ulmus davidiana, and *Quercus crispula* (Yazaki et al., 2016).

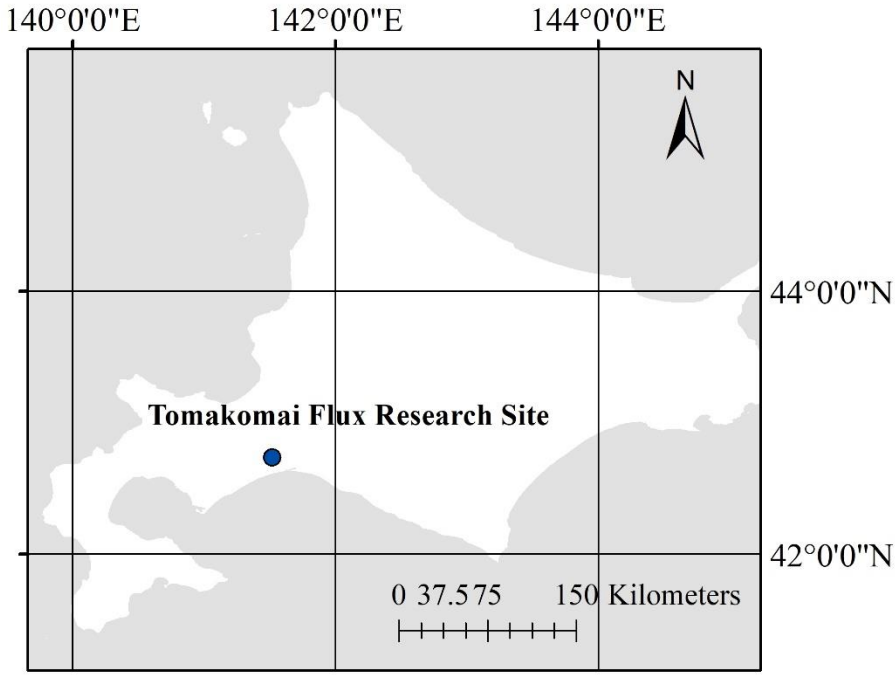


Figure 1. The location of Tomakomai Flux Research Site



Figure 2. The forest (Japanese larch plantation) in TMK site before typhoon Songda



Figure 3. The forest in TMK site was damaged by Typhoon Songda in 2004.



Figure 4. The forest in TMK site regenerated naturally in 2014.

II-2. SEIB-DGVM

II-2-1. Overview

SEIB-DGVM as a spatially explicit individual-based DGVM, calculates growth, competition and death of each tree with considering the environmental conditions of each tree in the spatially explicit virtual forest relative to the surrounding trees (Sato et al. 2007). There are three major calculation processes: physical, physiological, and vegetation dynamic processes (Appendix 1). They contain both mechanical-based and empirical-based algorithms. The physical processes contain day length, PAR, albedo, evaporation, transpiration, interception, runoff etc. Physiology contain photosynthesis, respiration, turnover, growth, phenology, decomposition etc. The physical and

physiological processes other than soil decomposition and tree growth are implemented at daily temporal step. Soil decomposition and tree growth is run at monthly step. Ecological dynamics processes calculate the establishment, competition, mortality, disturbance etc at annual step. Each individual tree is structured of three body parts: tree crown, tree trunk and fine root (Fig. 5). The crown and trunk of individual tree in SEIB was represented as a cylindrical shape. There are 10 layers inside the cylindrical of crown. The crown was simulated by leaf biomass ($mass_{leaf}$), leaf area (la), crown depth ($crwown_{depth}$) and crown diameter ($crwon_{diameter}$). The trunk contains two parts: sapwood and heartwood, which was simulated by diameters of sapwood ($dbh_{sapwood}$) and heartwood ($dbh_{heartwood}$), trunk biomass ($mass_{trunk}$), tree height ($height$) and lowest branch height. Both branch and coarse root biomass was included in trunk biomass. Fine root is formless and represented only by fine root biomass ($mass_{root}$).

II-2-2. Carbon cycle

Vegetation acquires carbon via photosynthesis by transforming the atmosphere carbon dioxide gas into organic matter. Assimilated carbon (carbohydrate) is used to support growth and maintenance respiration then recycled to the atmosphere as CO_2. At the end of the growing season leaves, root and dead trees produce litter, which is added to the litter pool. When the litter pool decomposes, 70% of the decomposed litter carbon is recycled to the atmosphere and remaining 30% carbon is added into the soil organic carbon pool 1 and 2 which has the fast decomposition rate and slow decomposition rate respectively. Finally, all decomposed soil organic carbon is released into the atmosphere as CO_2 (Fig. 6).

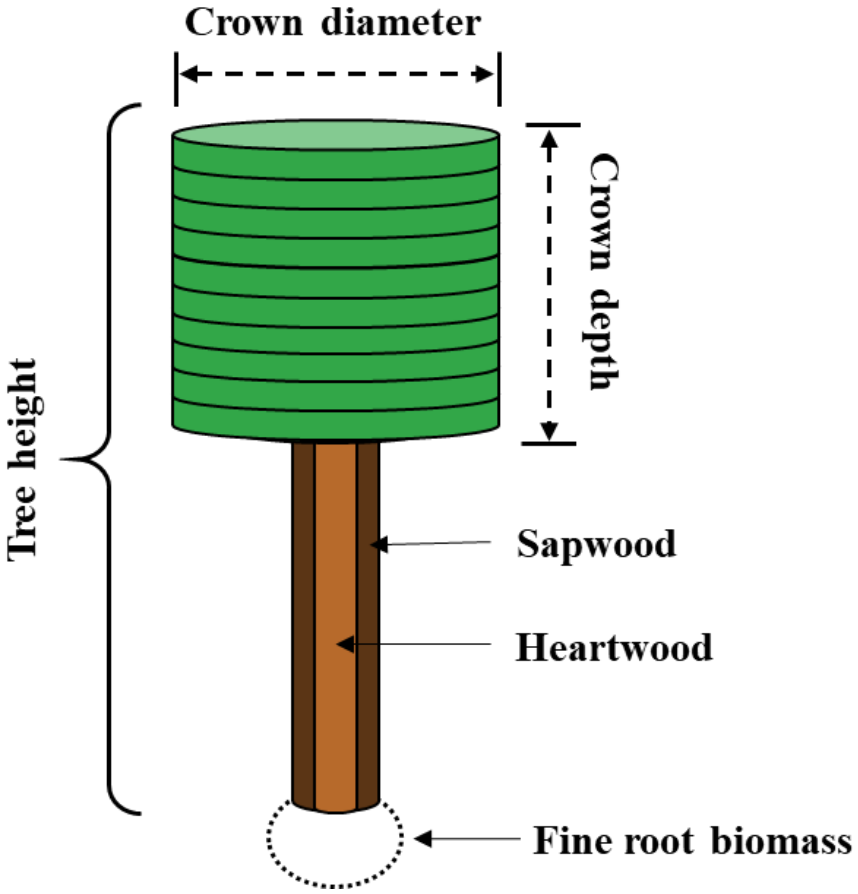


Figure 5. The representation of individual trees in SEIB-DGVM.

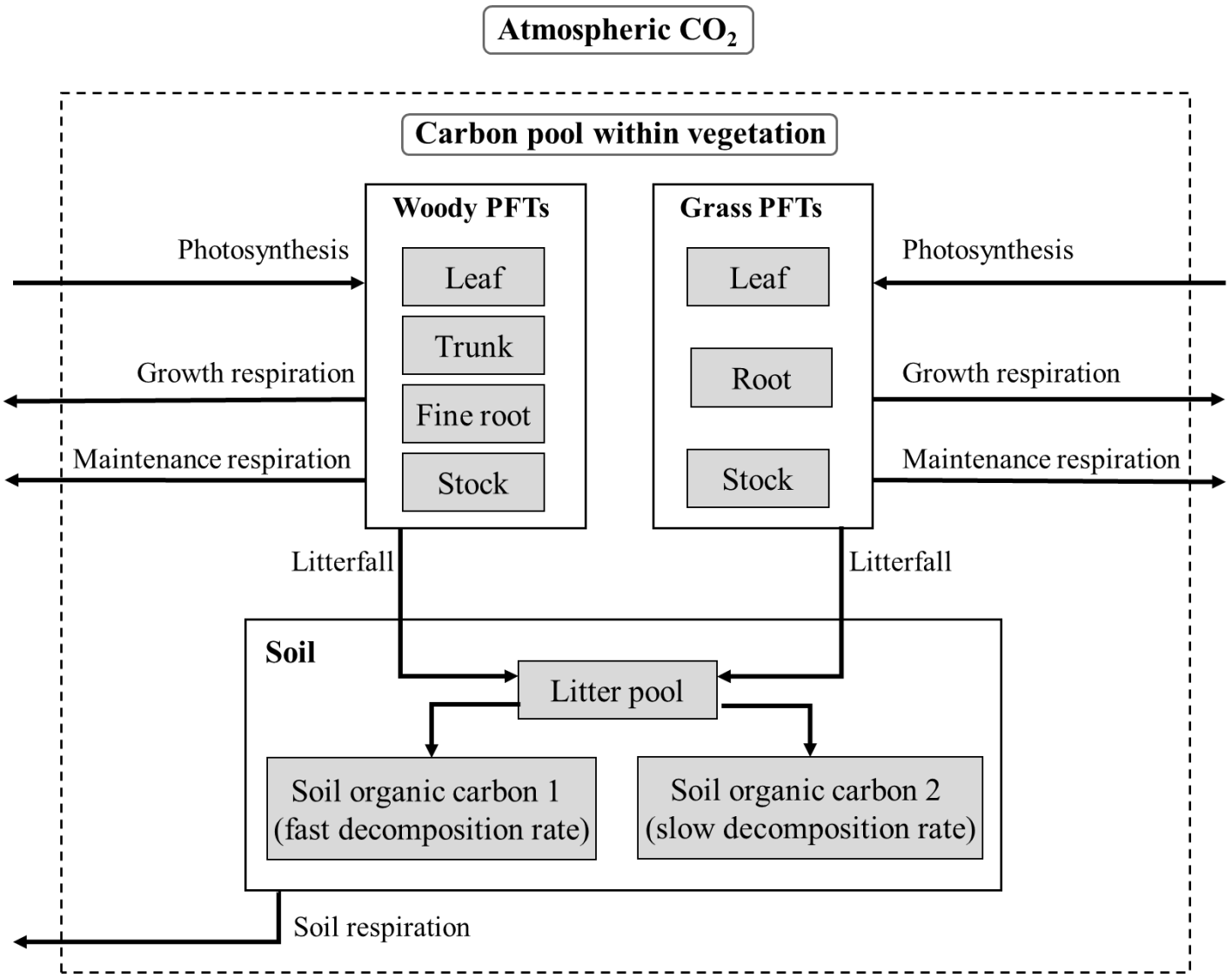


Figure 6. Carbon cycle in SEIB-DGVM

II-2-3. PAR

SEIB considered the light competition for individual tree in the virtual forest unit. Photosynthesis was calculated separately for each layer inside the tree crown. The midday photosynthetically active radiation (PAR) of each layer in each tree crown is calculated using the following formula:

$$par_{wood(l,n)} = fpar_{direct(l,n)} \times par_{direct} + fpar_{diffuse(l)} \times par_{diffuse} \quad (1)$$

where l is layer and n is tree number, $fpar_{direct(l,n)}$ and $fpar_{diffuse(l)}$ represent the absorbance of direct and diffuse of layer l of tree n compared to the forest top, respectively. The formula of $fpar_{direct(l,n)}$ and $fpar_{diffuse(l)}$ are as follow:

$$fpar_{direct(l,n)} = \exp\left(\frac{-1.0 \sum_{p=1}^{woody_pft}\left(EK_{(p)} la_{(p)}\right)}{crown_{area(n)}}\right) \quad (2)$$

$$fpar_{diffuse(l)} = \exp\left(-1.0 \sum_{p=1}^{woody_pft}\left(EK_{(p)} lai_{(l,p)}\right)\right) \quad (3)$$

Where *woody_pft* is the PFT for woody, $EK_{(p)}$ is vertical light attenuation coefficient of PFT p, $la_{(p)}$ is the sum of the leaf area of PFT p, $crown_{area(n)}$ is the cross section of the crown area of tree n, $lai_{(l,p)}$ is the leaf area index of layer l for PFT p.

II-2-4. Photosynthesis

Photosynthesis production of each layer *l* is calculated as follows:

$$gpp_{(l)} = 12 \times 10^{-6} \times 3600 \frac{1}{0.41505} la_{(l)} \int_0^{dlen} p_{single} dt$$

$$= 0.090936\ la_{(l)} dlen\ p_{sat} \left(1 - \frac{1}{\sqrt{1 + lue\ {par_{(l)}}/{p_{sat}}}} \right) \quad (4)$$

where constant number, $12 \times 10^{-6} \times 3600 \frac{1}{0.41505}$, is unit converter from (μ mol CO_2 $m^{-2}s^{-1}$) to (g DM $m^{-2}h^{-1}$), *dlen* is day length (hour), p_{sat} is the light saturated photosynthetic rate (Appendix 2), lue is the light use efficiency (Appendix 2), $par_{(l)}$is the intensity of PAR on layer *l* at midday. This formula is combined by Eqs. 5 and 6:

$$P_{single} = \frac{p_{sat}\ lue\ par}{p_{sat} + lue\ par} \quad (5)$$

$$x = par_l sin^2 \left(\pi \frac{t}{dlen} \right) \quad (6)$$

Where P_{single} is the single leaf photosynthetic rate, x is the intensity of PAR on crown layer *l* at time *t* (hour from sunrise).

II-3. Model setting

For all simulations, version 2.82 of SEIB-DGVM was employed (Sato et al., 2007, 2015), which is available online (http://seib-dgvm.com/data/seib_code282.zip). same parameter values were used as described in the appendix of Sato et al. (2007), except where noted below and in Appendix (3-7).

A spin-up simulation was conducted from the bare ground (no vegetation, no carbon) until soil carbon pools reached a quasi-equilibrium state for 1000 y. This site experienced two volcanic eruptions of Mt. Tarumae, in 1667 and 1739, which spread huge amounts of hot ash and are believed to have burnt most of the trees (Ujiie, 1984). Therefore, after the 1000 y spin-up procedure, AGB was removed once to a value of zero in 1667, and the spin-up was restarted for another 233 years (1667–1900) by repeatedly inputting the climatic data for 1901–1930 and constant atmospheric CO_2 concentration in 1900 (295 ppm) to SEIB-DGVM. Here the restart year of the spin-up was set once in 1667, although there could have been a second destructive eruption in 1739. Considering the long-term primary spin-up of 1000 years, however, the trend in our analysis in the later period would not show a large difference whether or not another removal of trees was added in 1739. After spin-up, four continuous simulation periods were set: historical (1901–1954), plantation (1955–2004), present (2005–2016), and future (2017–2100).

The original tree stand area of this model is 30 m × 30 m, the plot size normally used in regional and global simulations. The simulation in this study is a site scale simulation. If the plot is small, the possibility of occurrence of a large tree can create heterogeneity in forest structure and large variations in AGB. These variations can be averaged out at

large plot size, so the plot size was expanded to 100 m × 100 m. To better understand the direct impact of typhoons, the fire component of SEIB was turned off to exclude its impact.

SEIB-DGVM classifies the various functional traits of plant species into 16 PFTs aimed for practical use in global-scale simulation. In this study, plant species of the plantation period were aggregated into one woody PFT and two grass PFTs. Typhoon Toyamaru overturned or broke 90% of number of trees in 1954, when Japanese larch was planted at this site. So, there was an assumption that only boreal needle-leaved summer green trees are available during the plantation period. Forest type in the spin-up, historical, present, and future periods were set as natural mixed forest, so plant species were aggregated into five woody PFTs (temperate needle-leaved evergreen, temperate broad-leaved summer green, boreal needle-leaved evergreen, boreal needle-leaved summer green, and boreal broad-leaved summer green) and two grass PFTs (Sato et al., 2007). The settings for the five simulation periods are listed in Table 1.

Table 1. The settings for forest type, input climate data, and validation data source for the five simulation periods.

Period	Years	Forest Type	Climate Data	Validation Data
Spin-up	1667–1900	Natural mixed forest	CRU-TS3.22 NCEP/NCAR (harmonized with meteorological data at flux tower)	
Historical	1901–1954	Natural mixed forest	CRU-TS3.22 NCEP/NCAR (harmonized with meteorological data at flux tower)	
Plantation	1955–2004	Plantation (larch)	AMeDAS (harmonized with meteorological data at flux tower)	Hirano et al. (2003), Hirata et al. (2007)
Present	2005–2016	Natural mixed forest	Eddy flux data (Hirano et al., 2017)	Ide et al. (2011), Sano et al. (2010), Hirano et al. (2017)
Future	2017–2100	Natural mixed forest	MIROC-AGCM NCEP/NCAR (baseline, RCP2.6, and RCP8.5) (harmonized with meteorological data at flux tower)	

II-3-1. Leaf phenology for Japanese larch

Each deciduous tree species in the model has two phenological phases：growth and dormancy. Foliation and growth of deciduous trees occur only during the growing season. For the summer green needle leaved forest (BoNS), growth phase begins when the following two conditions are met: “soil temperature at 10 cm is greater than 5 ℃”, and “when the average air temperature of the day exceeds 0 ℃, the cumulative average daily temperature greater than 100 ℃ day”. Dormancy phase begins when the average temperature less than 7 ℃ for 10 days, leaf defoliation lasts 14 days, all leaves are converted into litter at a constant rate in this period. But this original phenology setting for deciduous needle-leaved trees, which was parameterized for the natural forest of larch in eastern Siberia, did not work well, the phenology scheme was modified to suit Japanese larch. The parameters were adjusted to initiate the leaf onset and offset to 1–10 May and 20–31 October, respectively; these dates were determined based on automatic photographs taken in 2001–2004 and 2011–2017. The photos were provided by the Center for Global Environmental Research, National Institute for Environmental Studies (http://db.cger.nies.go.jp/gem/en/flux/remo.html) via the Phenological Eyes Network database (http://pen.agbi.tsukuba.ac.jp). In this study, the initiating dates of leaf onset and offset was defined based on the cumulative daily air temperature above 5 ℃ of 270 ℃-day and that below 5 ℃ of -20 ℃ -day during the growing period (Ito et al., 2005).

II-3-2. Establishment

In SEIB-DGVM, woody PFTs emerge as a sampling of 1-cm Diameter at breast height (DBH) at the end of each simulation year. A woody PFT establishes at a constant rate at the end of each simulation year, if the following PFT-specific bioclimatic

conditions are satisfied: (1) the 20-yrs running mean of coldest-month temperature less than the maximum coldest-month temperature (TC_{max}); (2) the 20-yrs running mean of growing-degree day at 5 ℃ base (GDD) less than the maximum GDD (GDD_{max}); and (3) the 20-yrs running mean of GDD greater than minimum GDD (GDD_{min}). Additionally, for boreal broad-leaved summer green trees, it was assumed that establishment only occurs when the average midday photosynthetically active radiation in the previous year is greater than the minimum photosynthetically active radiation (PAR_{min}). For boreal needle-leaved summer green trees, it was originally assumed that they can only establish within 50 y of a wildfire. This assumption would be reasonable for larch in eastern Siberia but is not appropriate at this study site, where the fire rarely occurs. Because of our special focus on the effects of typhoons, the fire component was stopped due to the local history of no fire record, such that the larch establishment criteria for fire experience were removed. In SEIB-DGVM, the virtual forest is divided by a 1×1m grid mesh and each tree occupies one grid. This model assumes that the crowns of different trees cannot occupy the same space. Therefore, to establish a tree in a certain grid, the following two conditions must be satisfied: (1) there are no trees in this grid; (2) the newly established tree will not touch any trees which already exist in the adjacent grid. SEIB-DGVM assume that it has the same establishment rate ($P_{establish}$) for each grid which can establish a tree.

II-3-3. Mortality

The original tree mortality in SEIB-DGVM is calculated as the death rate for each individual tree on the last day of each simulation year. Mortality contains background mortality, heat stress, and bioclimatic limit. These are derived from the LPJ-DGVM (Sitch

et al., 2003). Background mortality is related to growth efficiency, which seems to be a sensitive indicator of resistance to environmental stress (Warning, 1983).In addition to these three different ways of mortality, there are several assumptions about mortality: (1) newly established trees will not die within the first two years; (2) the maximum longevity of woody PFT is assumed to be 200 years; (3) if the annual NPP of the previous year is negative, the background mortality rate of BoNS will increase by 10 times, while other woody PFT will die by 10% $year^{-1}$.

There was no tree mortality due to typhoon disturbance in the original model. In this study, from 1901 to 2016, the model was running by following the time and tree damage of the typhoons that have already occurred, those in 1954 and 2004, which damaged 100% and 90% of trees, respectively. To represent these stand-replacing disturbances, death rates of 100% and 90% of randomly selected trees are applied, respectively, at the ends of 1954 and 2004. It is difficult to precisely predict typhoon frequency and intensity in the future, so a sensitivity analysis was performed in the future period (2017–2100). In this study, typhoon frequency was represented by the number of typhoons and the typhoon intensity was represented by the percentage of tree mortality. As in the previous period, when each typhoon occurred, the simulation was suspended, randomly selected the specified percentage of trees from the virtual forest unit according to the specified typhoon intensity (tree mortality) and reduced the aboveground biomass (AGB) of these selected trees to zero, then continued to the subsequent simulation. The year, in which the typhoon occurred, was randomly selected (Appendix 8). The future period was divided into several parts according to the typhoon frequency and randomly selected one year as the typhoon year in each part. For example, when typhoons occur four times between

2017 and 2100, this 84-yrs period is equally divided into four 21-yrs periods, and a single typhoon event happens in a randomly selected year within each period (Appendix 8).

II-3-4. Scenario experiment design in the future

In the future period, 180 scenario experiments were conducted with the combinations of typhoon frequency (6 levels), typhoon intensity (10 levels), and climatic scenarios (3 scenarios; Fig. 7). Here, typhoon frequency and intensity were defined as the number of stand-replacing typhoons during the period 2017–2100 and as the removal percentage of tree stands due to the typhoon, respectively. The typhoon frequency was given by six ranks, 1, 2, 4, 8, 16, and 20 times over the 84 y (2017–2100), and typhoon intensity was given by 10 levels ranging from 10% to 100% at 10% intervals. Considering the full range of typhoon frequency from zero per year to yearly would have required a great deal of calculations, so frequency was limited to these six ranks. To avoid several typhoons occurring in same year, the future period was divided (2017–2100) into 1, 2, 4, 8, 16, and 20 parts, and then randomly selected one year from each part as the typhoon year.

Each of the 180 scenario experiments was associated with 10 ensembles (iterations) with typhoons striking at different years and different tree stand positions decided by random numbers. For example, for the scenario with a frequency of 2 and an intensity of 10%, SEIB-DGVM was run 10 times with two randomly selected years from 2017 to 2100 with a typhoon strike, and the AGB (consisting of a crown, trunk, and fine roots) was removed at the end of the typhoon year for 10% of randomly selected tree stands. This removal scheme assumes that all trees damaged by a typhoon are uprooted and their

carbon stock is lost from the study plot, which was based on the management policy after typhoon Songda.

Three types of climate forcing data were input in this study: baseline and Representative Concentration Pathways (RCP) 2.6 and RCP8.5 in the future period (2017–2100), with the same typhoon scenario and model setting used in each. The baseline experiment was conducted to provide a baseline reference for comparison with RCP2.6 and RCP8.5 by repeatedly inputting 20 years of climate data (1997–2016) and inputting the global averaged annual mean atmospheric CO2 value in 2016 (402.8 ppm). There are four pathways which have been selected for climate modeling and research. RCP 2.6 is a very low forcing level (Van Vuuren et al., 2011c). RCP 4.5 and 6 are two medium stabilization scenarios. RCP 8.5 is a very high baseline emission scenario (Riahi et al., 2011). In this study, the two extreme scenarios were selected: RCP 2.6 and 8.5. Overall, our study included 1800 runs with 60 typhoon scenarios × 10 iterations × 3 climate forcings (Fig. 7).

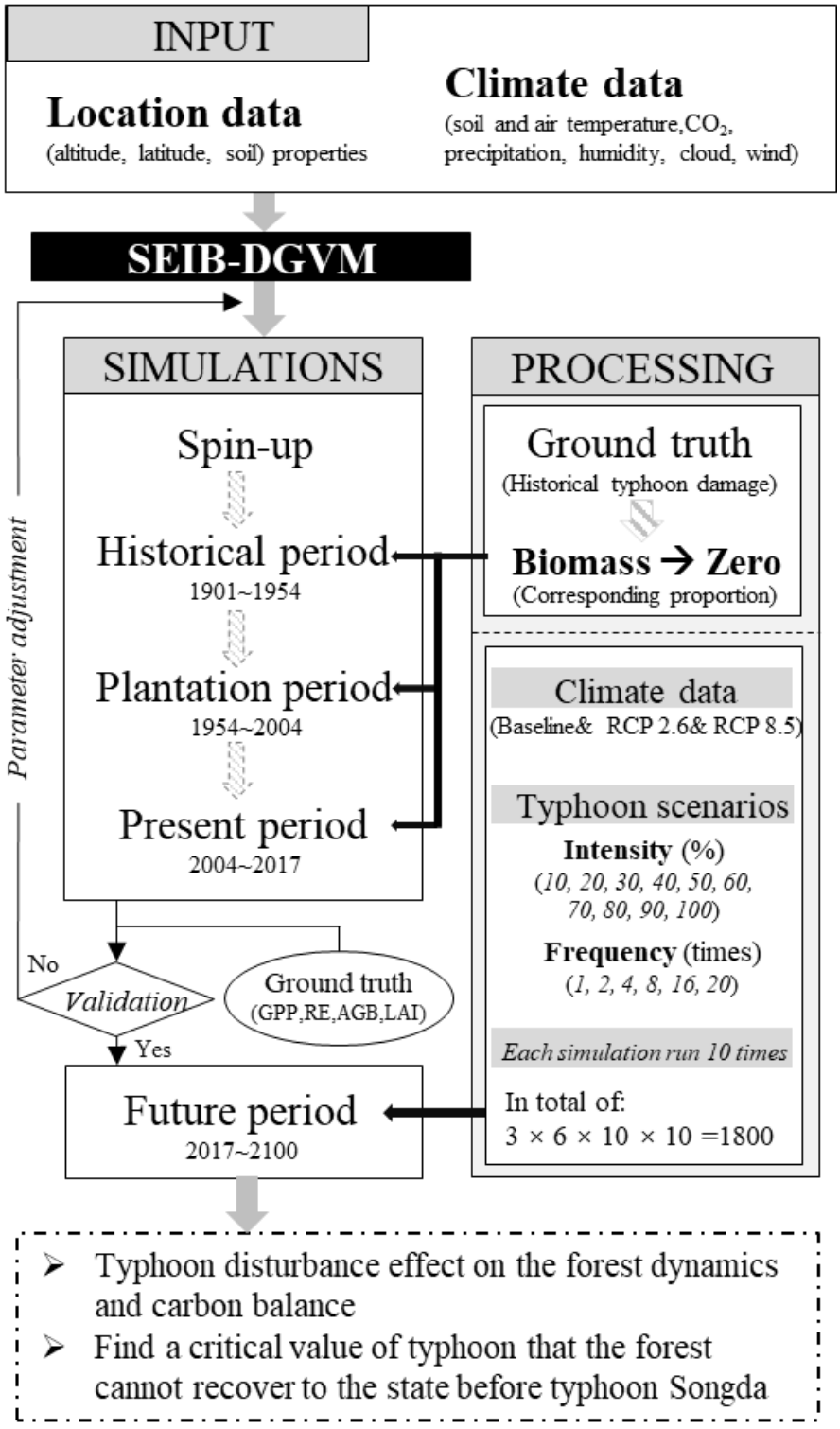


Figure 7. Flow chart of the simulation runs

II-4. Climate data

II-4-1. Input data of SEIB-DGVM

SEIB-DGVM (version 2.82) requires the following nine daily meteorological variables: surface air temperature (°C), soil temperatures at 0–10 cm depth (°C), soil temperatures at 10–200 cm depth (°C), soil temperatures at 300 cm depth (°C), precipitation (mm day^{-1}), total cloudiness (fraction), wind velocity (m s^{-1}), specific humidity (kg kg^{-1}), and daily range of surface air temperature (°C).

II-4-2. Climate data sources at different simulation periods

In the historical period (1901–1954), the observation-based climate data synthesized from CRU TS3.22 (Climate Research Unit Times-Series Version 3.22; Harris et al., 2014) and re-analysis climate data NCEP/NCAR (National Center for Environmental Prediction/National Center for Atmospheric Research) was used. Monthly CRU data were supplemented by daily climate variability within each month, using the NCEP/NCAR data (Kalnay et al., 1996). A simple linear interpolation was applied to harmonize the climate from these coarse climate data (0.5 × 0.5 degrees for CRU, 2 × 1.75 degrees in global for NCEP/NCAR) to that of the study site (Sato et al., 2007). In the plantation period (1955–2004), AMeDAS climate data provided by the Japan Meteorological Agency (http://www.data.jma.go.jp/gmd/risk/obsdl/index.php) was used. Because AMeDAS has no soil temperature data, CRU TS3.22 NCEP/NCAR data was used to replaced them. In the present period (2005–2016), the flux-tower observation data (Hirano et al., 2017) was used. In the future period (2017–2100), the climate scenarios provided by the Model for Interdisciplinary Research on Climate (MIROC) Atmospheric General Circulation Model (AGCM) output under the RCP2.6 and RCP 8.5 scenarios (K-

1 Model Developers, 2004, Emori et al., 2005, Watanabe et al., 2011, Hajima et al., 2012) was used.

To retain consistency among climate data, the climate data of different sources was harmonized to that of flux-tower data by using linear regression during the years of data overlap. Information on the input climate data sources is listed in Fig. 8. The SEIB-DGVM website provides an online system that generates meteorological data for model input from 1901 to 2013. This climatic data generator is based on CRU TS3.22 and NCEP/NCAR data. CRU TS3.22 observation-based data are monthly, but SEIB-DGVM requires daily climate data, so this system used the National Centers for Environmental Prediction/National Center for Atmospheric Research (NCEP/NCAR) daily climate data to provide daily climatic variability within each month. Detailed data descriptions are available at http://seib-dgvm.com/data_server2.html. After entering the latitude and longitude on this online system, the meteorological data that are in accordance with the SEIB input data format can be downloaded. The spatial resolution of this data is 0.5 degree.

For global simulation, though the abovementioned data is feasible, it may be less accurate for site scale simulation. So, more accurate Tomakomai flux-tower data (2005–2017) and AMeDAS data (1954–2004) was used instead. AMeDAS did not observe soil temperatures, so the soil temperature (1954–2004) was from the online system generator. AMeDAS has no record on total cloudiness, wind velocity, and specific humidity from 1954 to 1960, so these data were downloaded from the online system (http://seib-dgvm.com/data_server2.html).

II-4-3. Validation data

Validation data were obtained from observation studies: annual woody AGB and annual woody leaf area index (LAI) for 2006, 2007, 2009, and 2011–2014 were from Yazaki et al. (2016) and monthly gross primary production (GPP) and RE from September 2000 to August 2001 were from Hirano et al. (2003). Monthly GPP and RE from April to December in 2005–2015 were from Hirano et al. (2017).

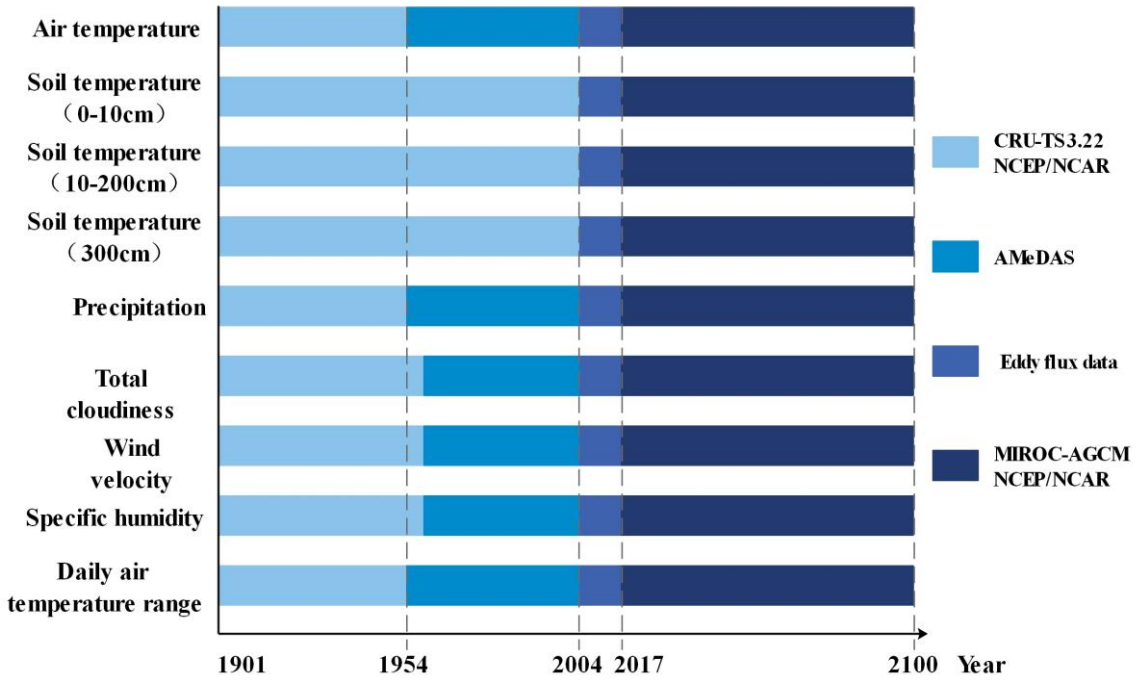


Figure 8. Input climate data source. Vertical is the timeline, horizontal is the 9 meteorological variables that need to be input to SEIB-DGVM. Different colors represent different data sources.

III. Results

Ⅲ-1. Model validation

SEIB-DGVM reproduced the observed interannual variations at the Tomakomai Flux Research Site before and after typhoon Songda. GPP and RE before the typhoon were only slightly overestimated, but kept high correlation coefficients (R^2 = 0.80 and 0.89; Fig. 9). After typhoon Songda, GPP (R^2 = 0.55) and RE (R^2 = 0.61) were well represented (Fig. 10). The model also reconstructed the AGB (R^2 = 0.63) and LAI (R^2 = 0.77) well after typhoon Songda, but there was a slightly underestimated (Fig.11).

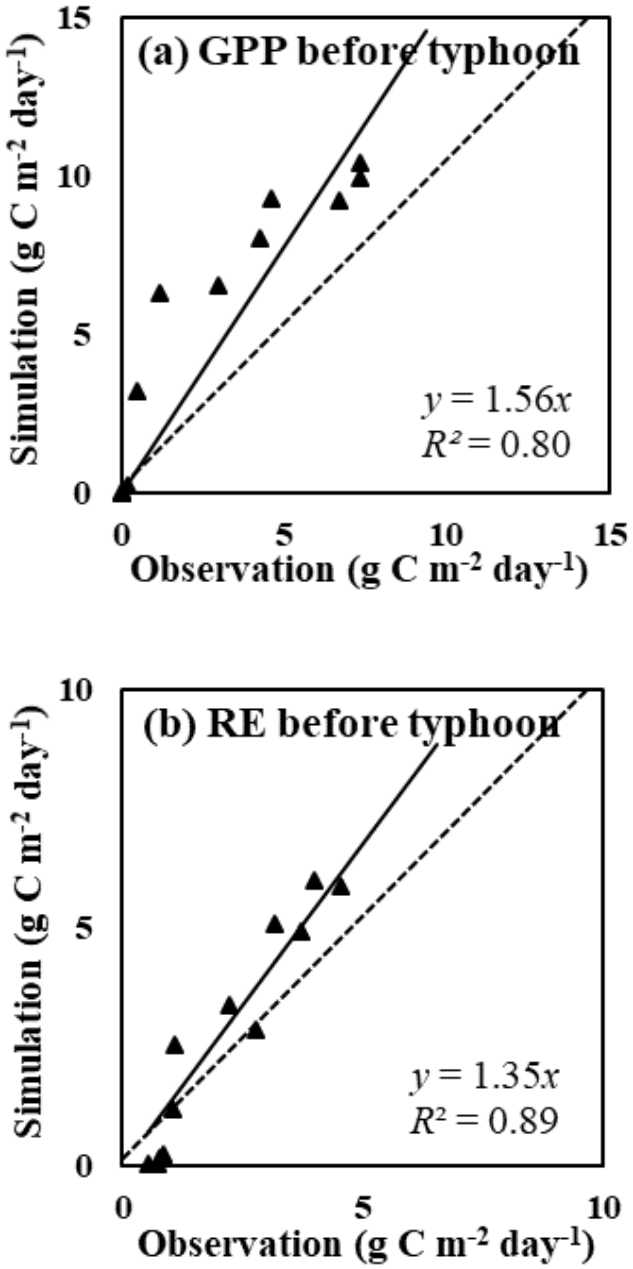


Figure 9. Validation result before typhoon Songda in 2004. (a) Scatter plots between observation and simulation for monthly mean GPP; (b) Monthly mean RE.

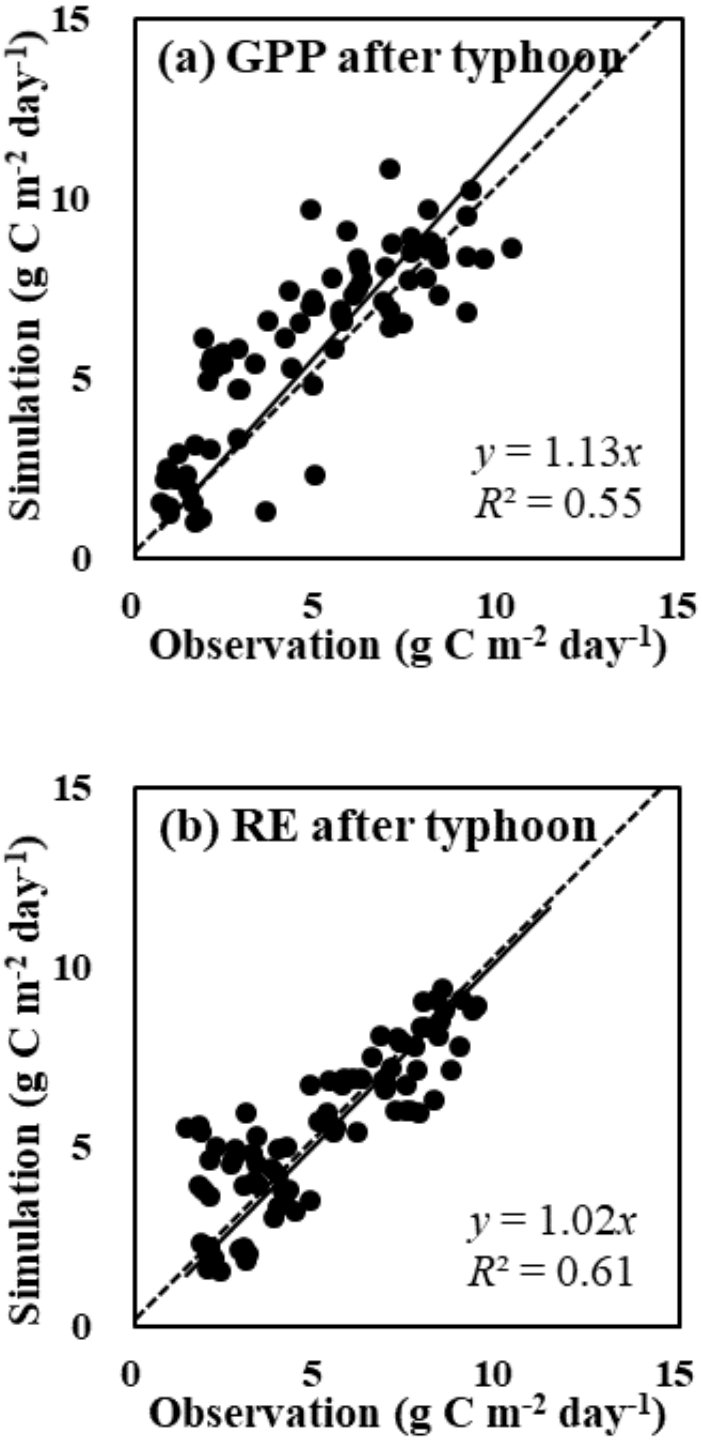


Figure 10. Validation result after typhoon Songda in 2004. (a) Scatter plots between observation and simulation for monthly mean GPP; (b) Monthly mean RE.

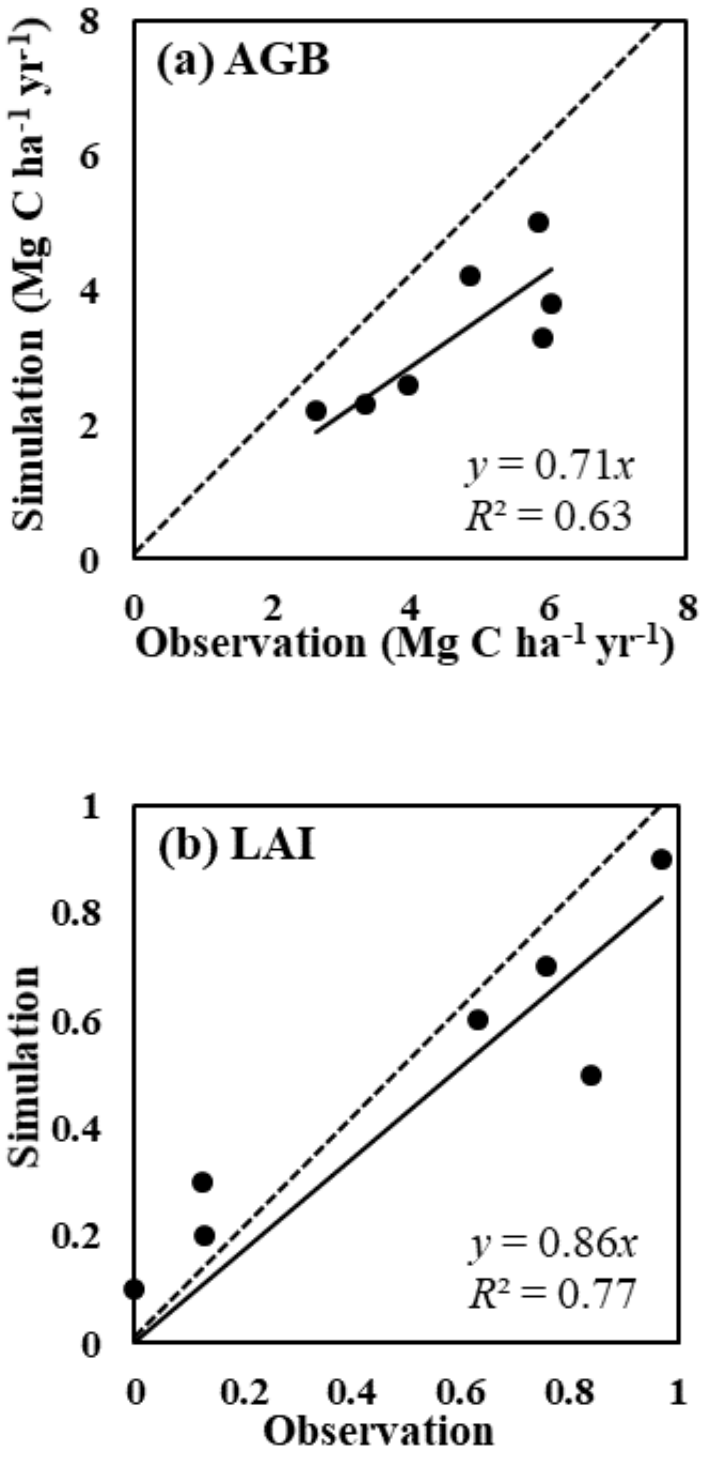
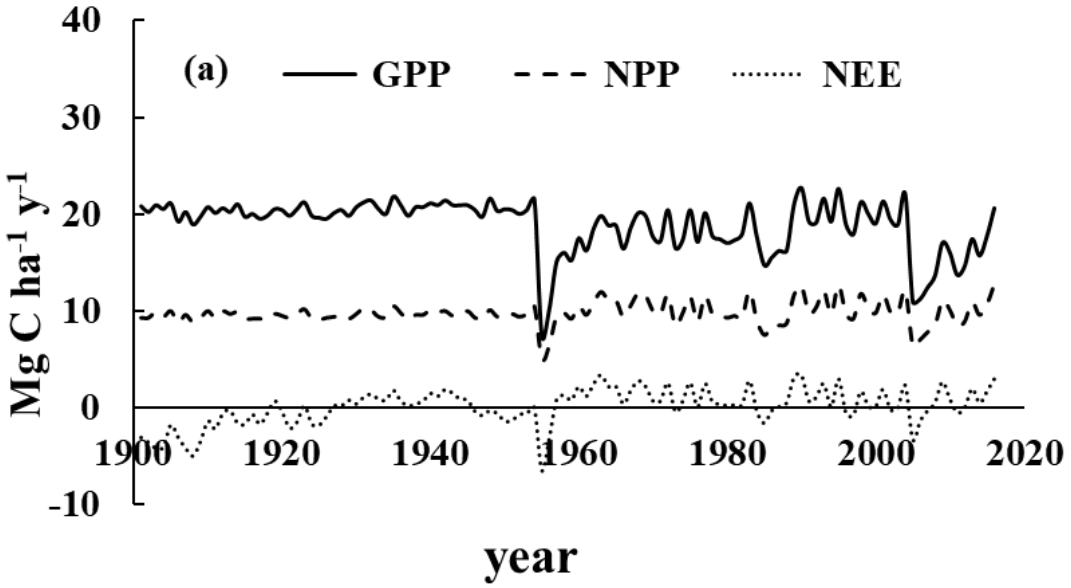


Figure 11. Validation result after typhoon Songda in 2004. (a) Scatter plots between observation and simulation for annual AGB; (d) Annual LAI.

III-2. Variations of carbon and forest dynamics in the past

The long-term variation in carbon and forest dynamics was simulated for 1901–2016 (Fig. 12). During 1901–1954, the mixed broad-leaved–conifer forest grew at the site. The average annual GPP, net primary production (NPP), and NEP were 20.4, 9.6, and –0.7 Mg C ha^{-1} y^{-1}, respectively, and averaged annual tree height and DBH were 6.5 m and 9.1 cm. This phase can be regarded as the equilibrium state of naturally regenerated forest under the baseline climatic condition. After the typhoon in 1954, the forest type was artificially converted into a larch plantation, and GPP, NPP, tree height, and DBH showed a considerable decrease and then a gradual recovery until the 1970s. After that, all variables were stabilized and close to those prior to the 1954 typhoon. In 2004, a typhoon completely destroyed the larch plantation, and since then the mixed forest has been recovering naturally. By 2017, the values of GPP and NPP had recovered to those prior to the typhoon, but tree height and DBH were still lower.



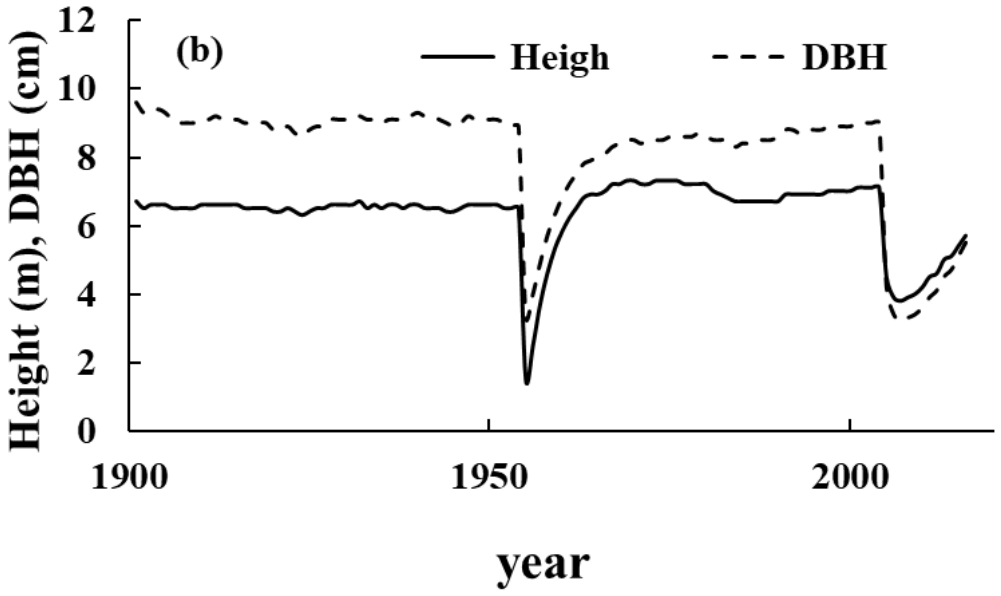


Figure 12. Simulation results from 1901 to 2016: (a) GPP, NPP, and NEP (Mg C ha^{-1} y^{-1}) and (b) tree height (m) and DBH (cm).

III-3. Effect of typhoons on forest structure in the future

Figure 13-18 shows the time series of simulated AGB from 2017 to 2100 under the baseline, RCP2.6, and RCP8.5 scenarios. The average woody AGB in the last decade of the 21st century ranged from 0.78 to 118 Mg C ha^{-1} in RCP 2.6 (Fig.16 b) and from 0.8 to 136 Mg C ha^{-1} in RCP8.5 (Fig.18 b) as the frequency and intensity of typhoons increase from 1 to 20 times per 84 y and from 10% to 100%, respectively. The woody AGB time series from 2017 to 2100 shows a significant decrease with increasing typhoon frequency and intensity ($p < 0.01$) under both RCP 2.6 and RCP 8.5. Of note, at a typhoon intensity of 100%, the forest will not be able to recover back to the pre-typhoon AGB (90.6 Mg C ha^{-1}) under any frequency for the baseline and RCP 2.6 scenarios. The bar chart in Figure 16.b and 18.b are the average AGB from 2091 to 2100 for all typhoon scenarios; under RCP 2.6 and RCP 8.5, when typhoon frequency is ≤ 2 and intensity is $\leq$ 40%, the average value of AGB at the end of the 21st century is greater than that pre-typhoon.

During the scenario simulation from 2017 to 2100, there were also significant effects of typhoon frequency and intensity on tree height, woody LAI, and grass LAI. Figure 19 and 20 are the three-dimensional surface counter figure showing the effect of typhoon frequency and intensity on forest traits. As both typhoon frequency and intensity increase, woody AGB (Fig.19 a), tree height (Fig.19 b), and woody LAI (Fig.20 b) decrease, whereas grass LAI (Fig.20 a) increases.

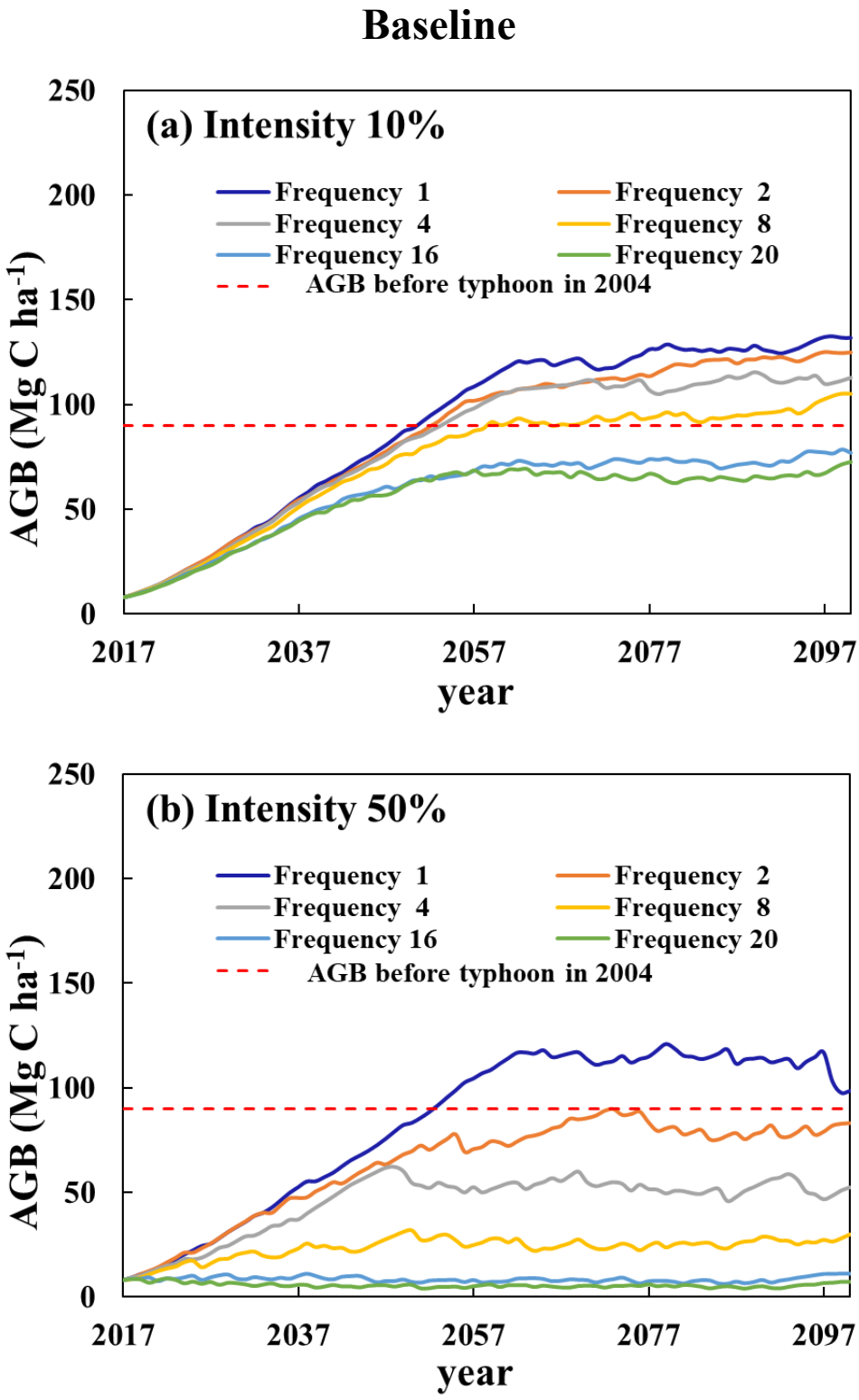


Figure 13. Aboveground woody biomass (AGB) simulated in the **baseline scenario** in the case of typhoon intensity of (a) 10% and (b) 50% from 2017 to 2100.

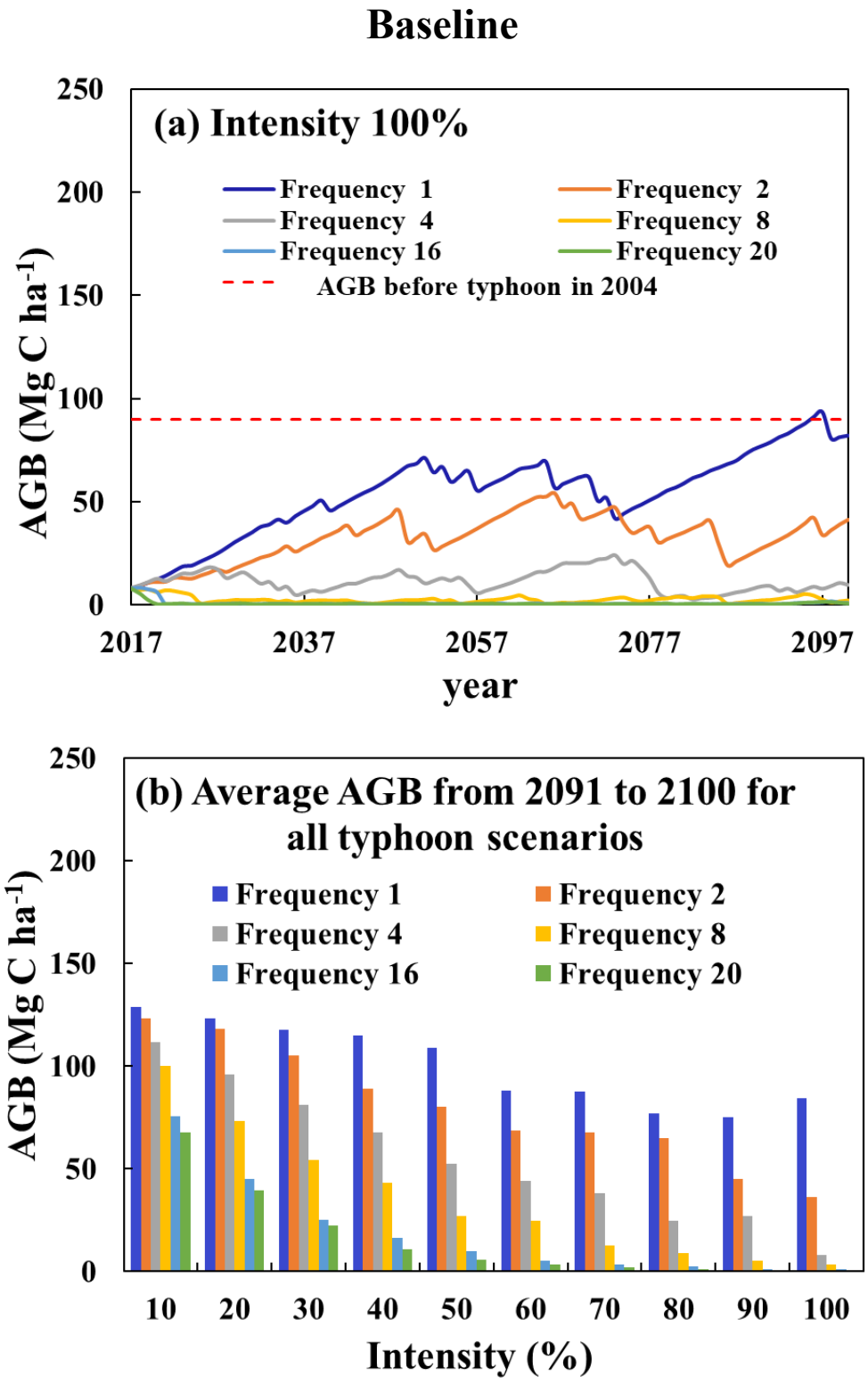


Figure 14. Aboveground woody biomass (AGB) simulated in the **baseline scenario** in the case of typhoon intensity of (a) 100% from 2017 to 2100 and (b) average AGB in last decade (2091–2100) for all typhoon scenarios.

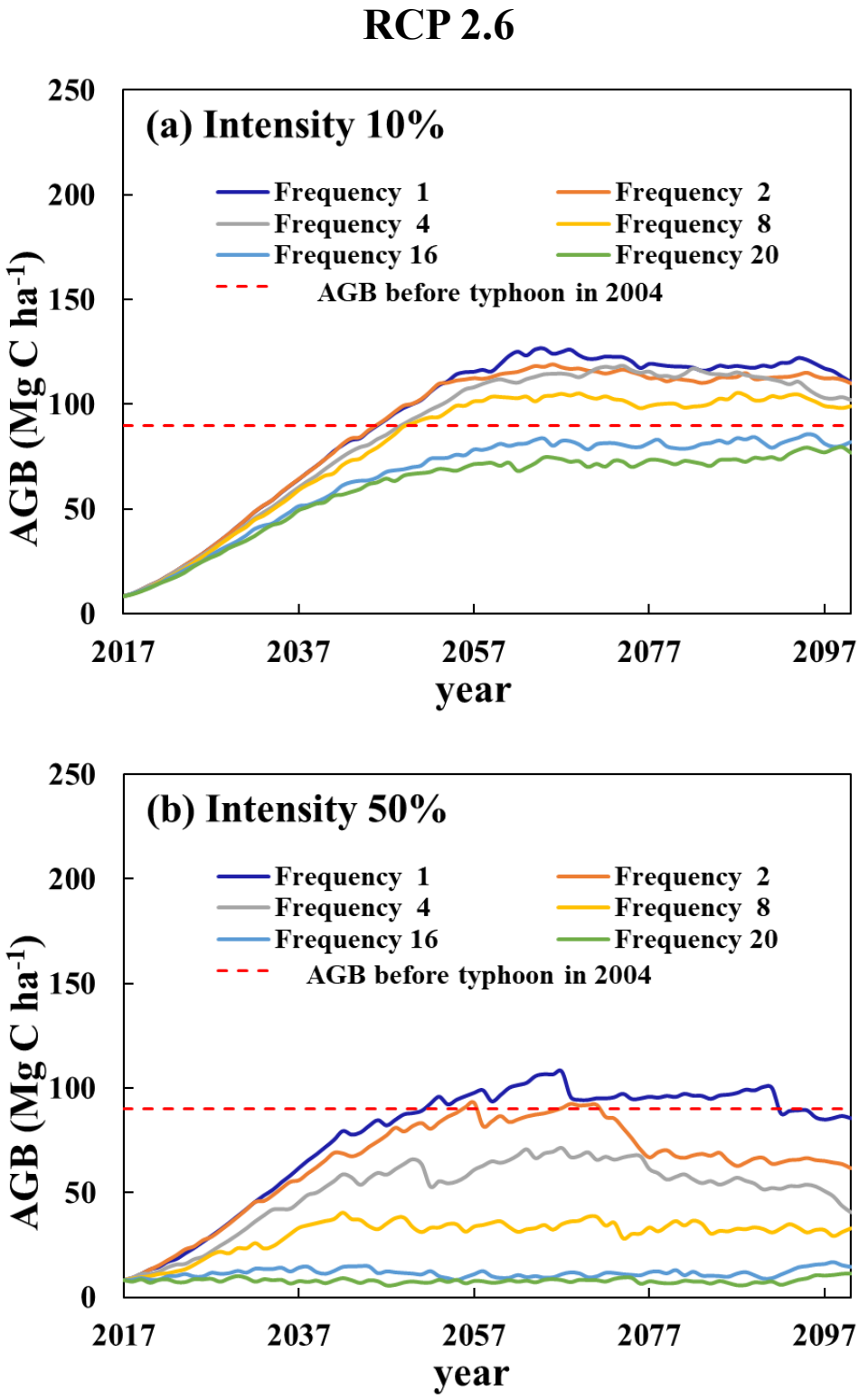


Figure 15. Aboveground woody biomass (AGB) simulated in the **RCP 2.6 scenario** in the case of typhoon intensity of (a) 10% and (b) 50% from 2017 to 2100.

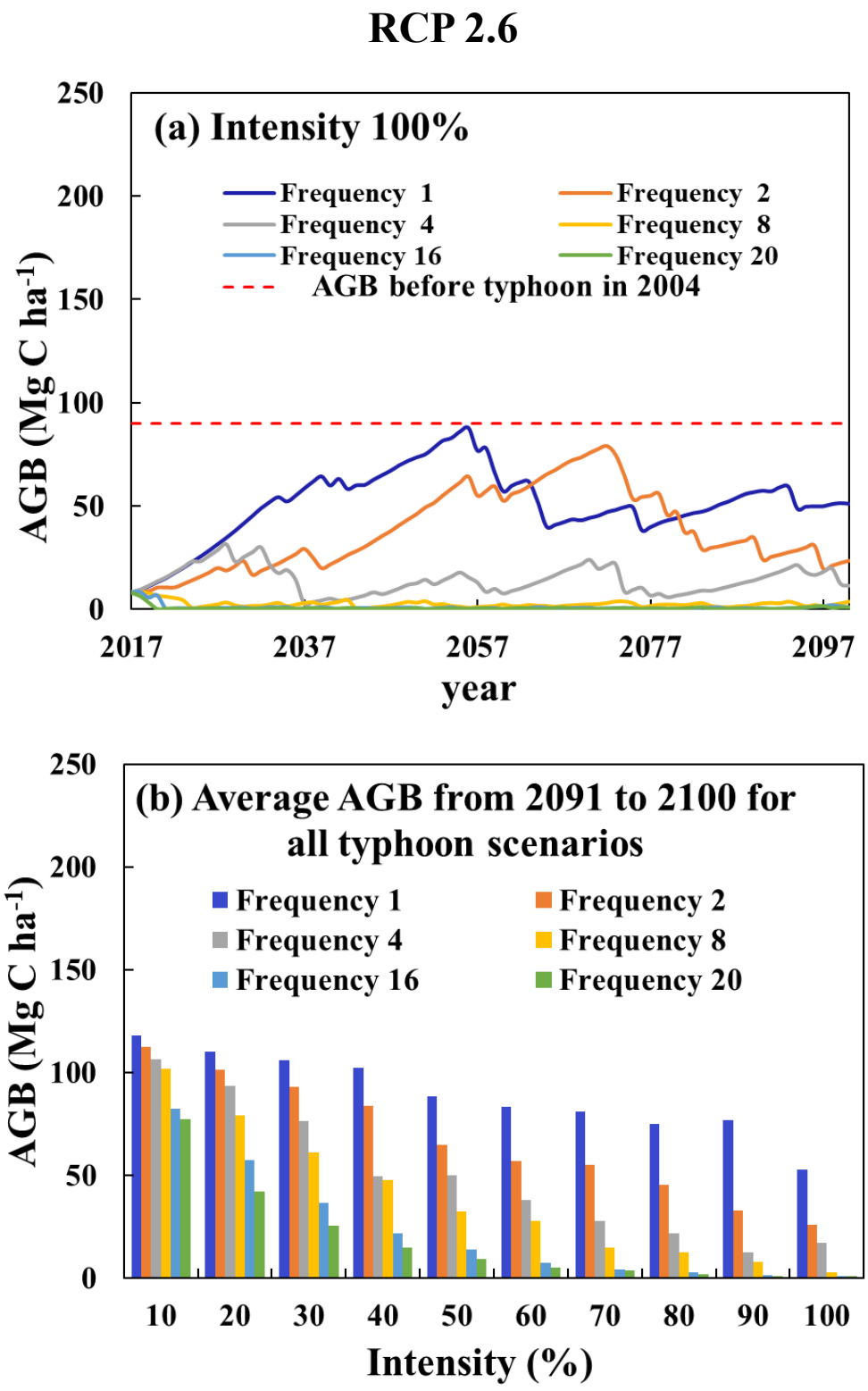


Figure 16. Aboveground woody biomass (AGB) simulated in the **RCP 2.6 scenario** in the case of typhoon intensity of (a) 100% from 2017 to 2100 and (b) average AGB in last decade (2091–2100) for all typhoon scenarios.

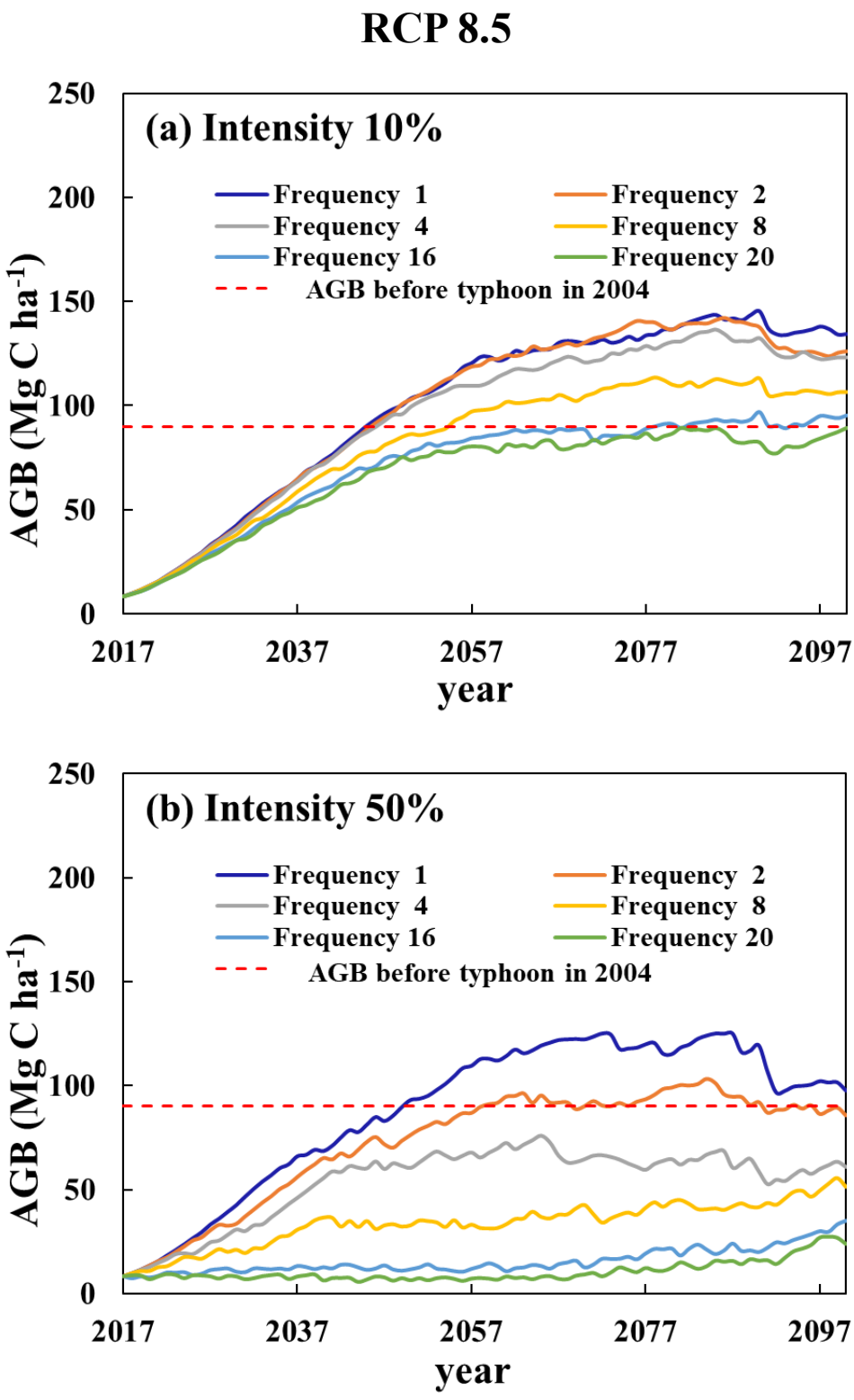


Figure 17. Aboveground woody biomass (AGB) simulated in the **RCP 8.5 scenario** in the case of typhoon intensity of (a) 10% and (b) 50% from 2017 to 2100.

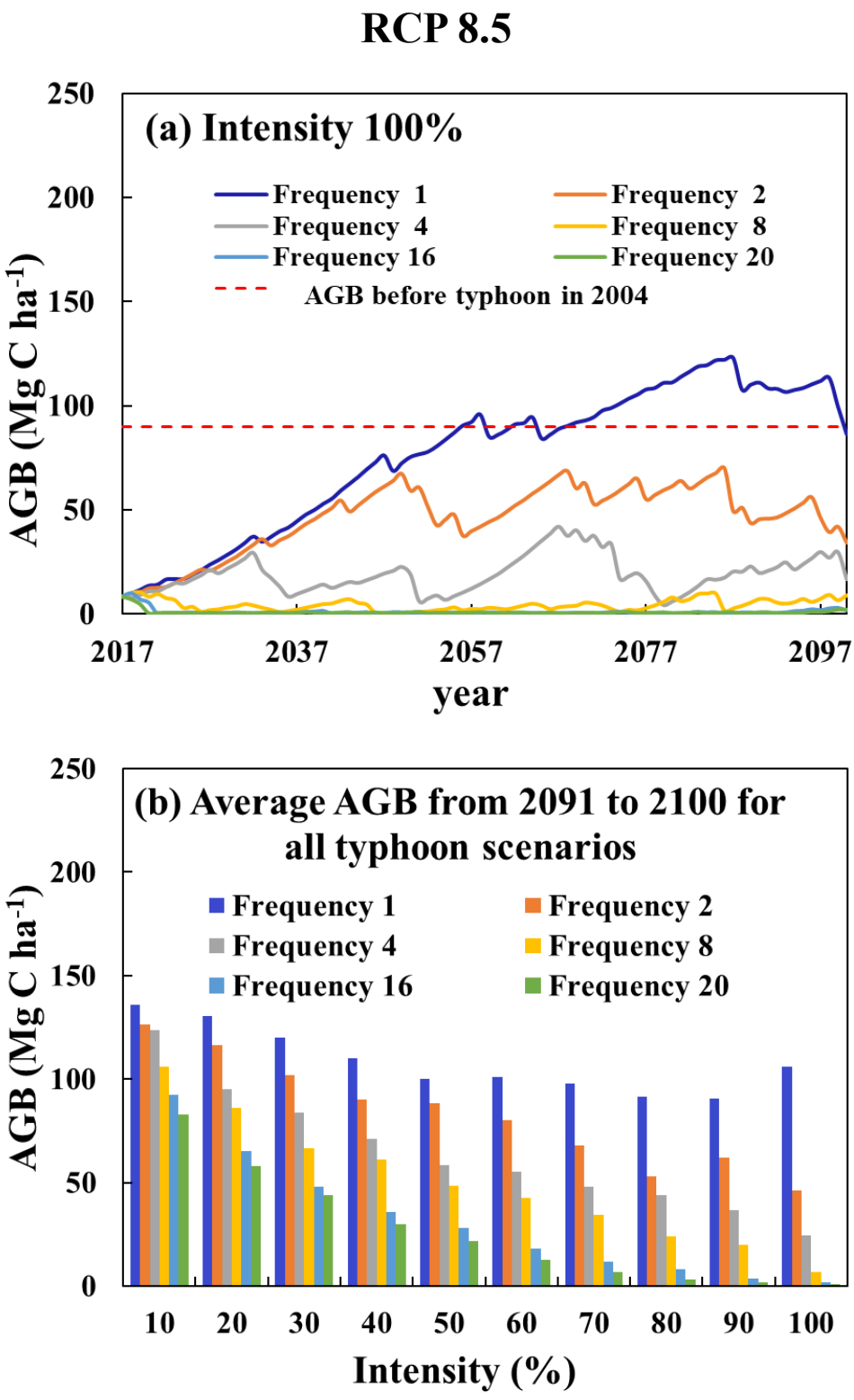


Figure 18. Aboveground woody biomass (AGB) simulated in the **RCP 8.5 scenario** in the case of typhoon intensity of (a) 100% from 2017 to 2100 and (b) average AGB in last decade (2091–2100) for all typhoon scenarios.

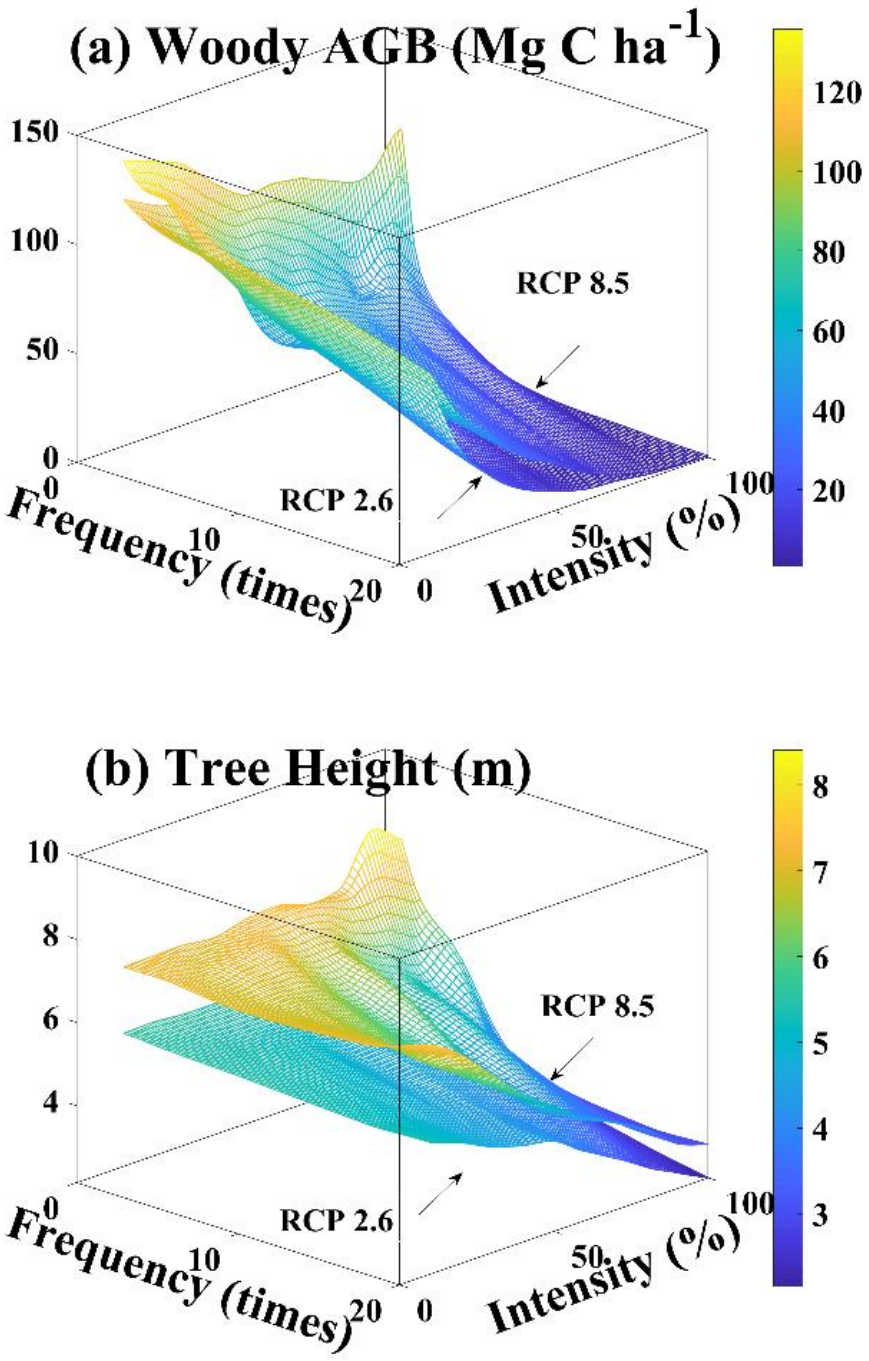


Figure 19. The effect of typhoon frequency and intensity on (a) woody AGB and (b) tree height under RCP2.6 and RCP8.5 scenarios. Values are average for the last decade of the 21st century (2091–2100). The color bar on the right-hand side for each figure shows the range for each variable. The colors from yellow to blue represent the high value to low value for each variable.

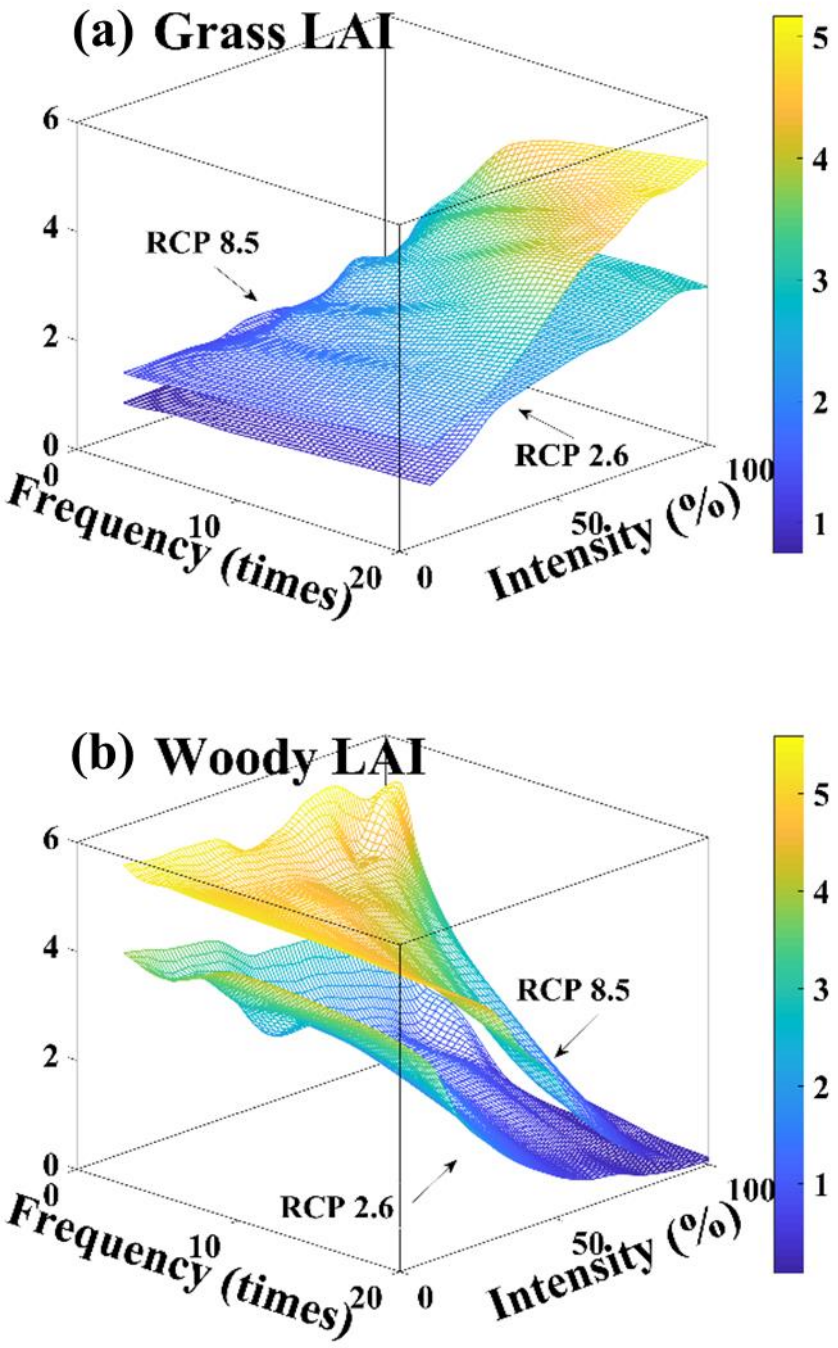


Figure 20. The effect of typhoon frequency and intensity on (a) mean LAI of grass and (b) mean LAI of woody plants under RCP2.6 and RCP8.5 scenarios. Values are average for the last decade of the 21st century (2091–2100). The color bar on the right-hand side for each figure shows the range for each variable. The colors from yellow to blue represent the high value to low value for each variable.

Ⅲ-3. Effect of typhoons on carbon dynamics

As with the AGB results, the interannual changes in NPP and NEP show significant relationships with increasing typhoon intensity and frequency under both RCP2.6 and RCP8.5 ($p < 0.01$, Fig. 22 a and b). Compared to the typhoon frequency, increasing typhoon intensity causes the steeper NPP decline. As typhoon frequency and intensity increase, NEP first increases and then decreases. Soil organic matter (Fig. 21 a), litter (Fig. 21 b), and heterotrophic respiration (Fig. 23) show a similar decline with increasing typhoon frequency and intensity.

Figures 24-29 shows the NPP time series from 2017 to 2100 for different typhoon conditions under the baseline, RCP 2.6, and RCP 8.5 scenarios. At baseline, NPP shows a relatively constant transition. Under the RCP 2.6 scenario, NPP first increases and then decreases slightly in most of the simulations. Under the RCP8.5 scenario, NPP increases gradually in all of the simulations. The average NPP of the last decade was also considered. At baseline, when frequency is $\geq$ 16, the impact of a typhoon becomes apparent when intensity is $\geq$ 30%. When frequency ranges from 4 to 8, if the intensity is < 50%, there will not be a significant typhoon effect. When frequency is $\leq$ 2, the typhoon will have little impact on the final NPP. Under the RCP2.6 scenario, when intensity is $\leq$ 20%, the less frequent typhoons are the greater their influence on NPP. When intensity is $\geq$ 30%, the impact of high-frequency typhoons becomes significant, whereas for low-frequency typhoons the impact will become apparent when the corresponding intensity is $\geq$ 50%. Under the RCP 8.5 scenario, only when intensity is $\geq$ 60% and the corresponding frequency is $\geq$ 16 the impact of typhoons on the average final NPP will be obvious.

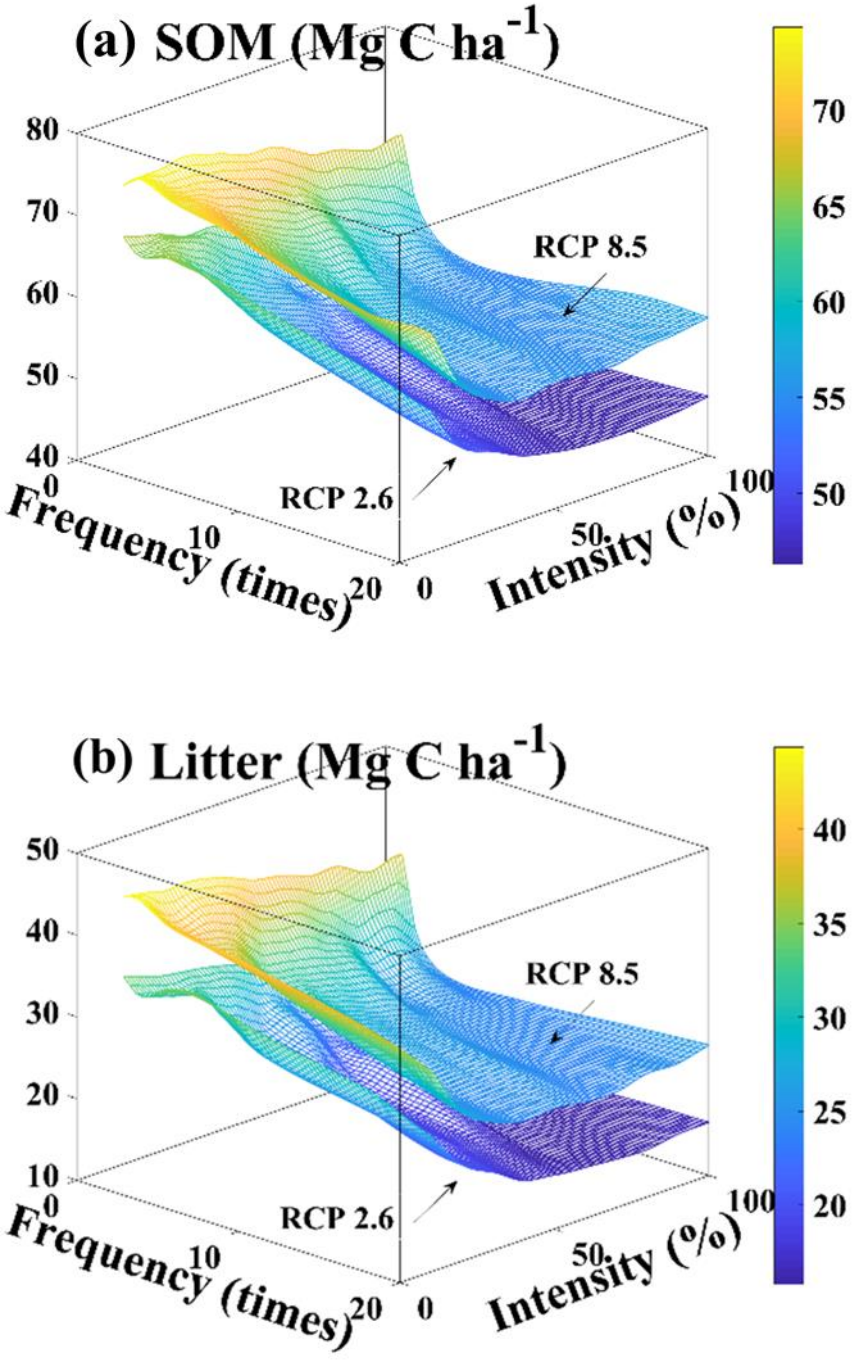


Figure 21. The effect of typhoon frequency and intensity on (a) SOM (soil organic matter) and (b) litter under RCP2.6 and RCP8.5 scenarios. Values are average for the last decade of the 21st century (2091–2100). The color bar on the right-hand side for each figure shows the range for each variable. The colors from yellow to blue represent the high value to low value for each variable.

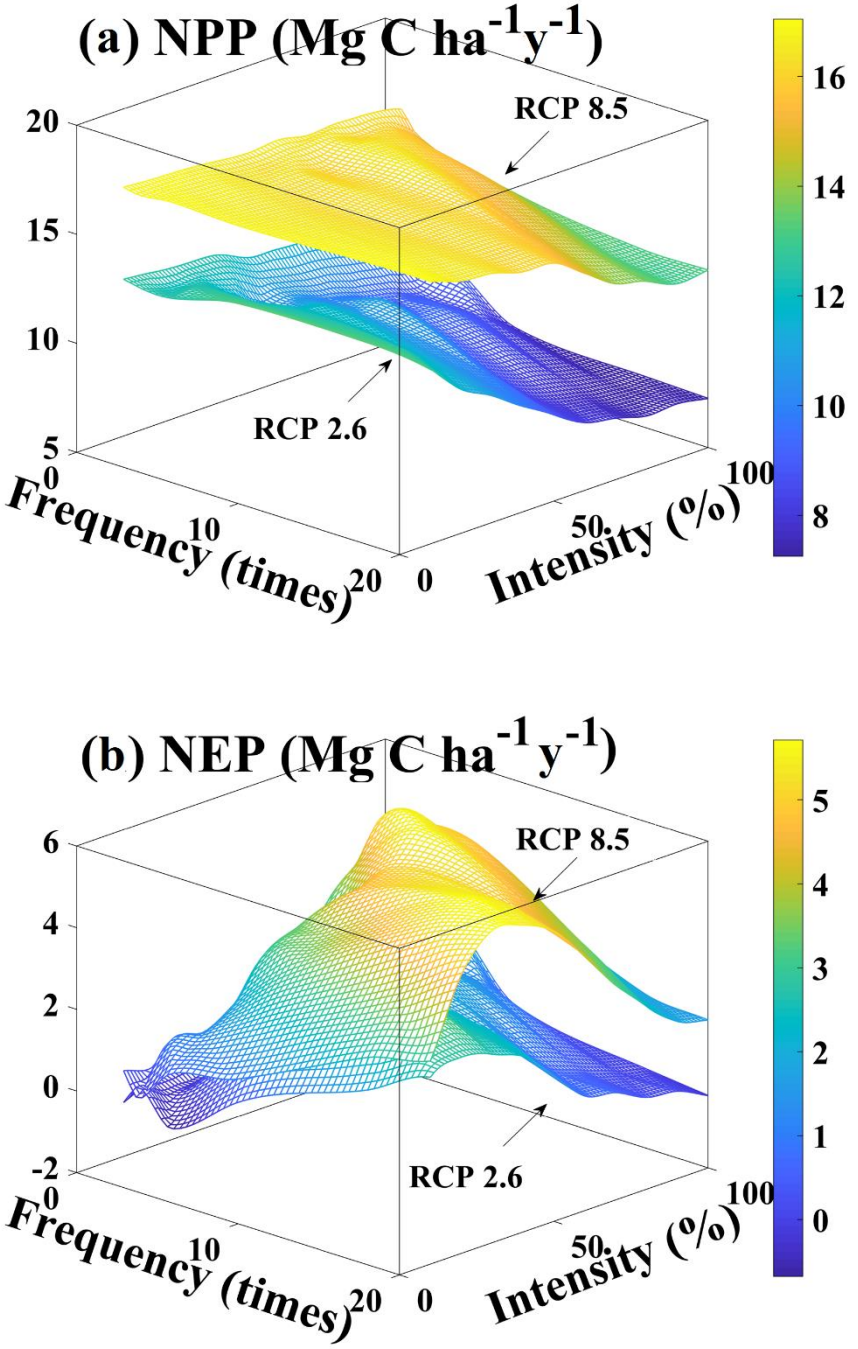


Figure 22. The effect of typhoon frequency and intensity on (a) NPP and (b) NEP under RCP2.6 and RCP8.5 scenarios. Values are average for the last decade of the 21st century (2091–2100). The color bar on the right-hand side for each figure shows the range for each variable. The colors from yellow to blue represent the high value to low value for each variable.

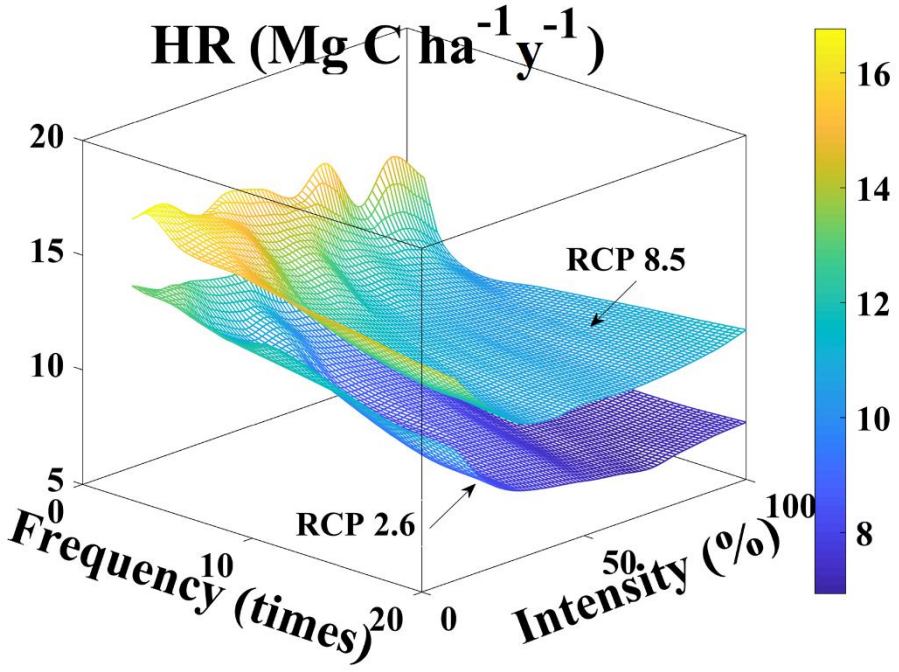


Figure 23. The effect of typhoon frequency and intensity on heterotrophic respiration (HR) under RCP2.6 and RCP8.5 scenarios. Values are average for the last decade of the 21st century (2091–2100). The color bar on the right-hand side for each figure shows the range for each variable. The colors from yellow to blue represent the high value to low value for each variable.

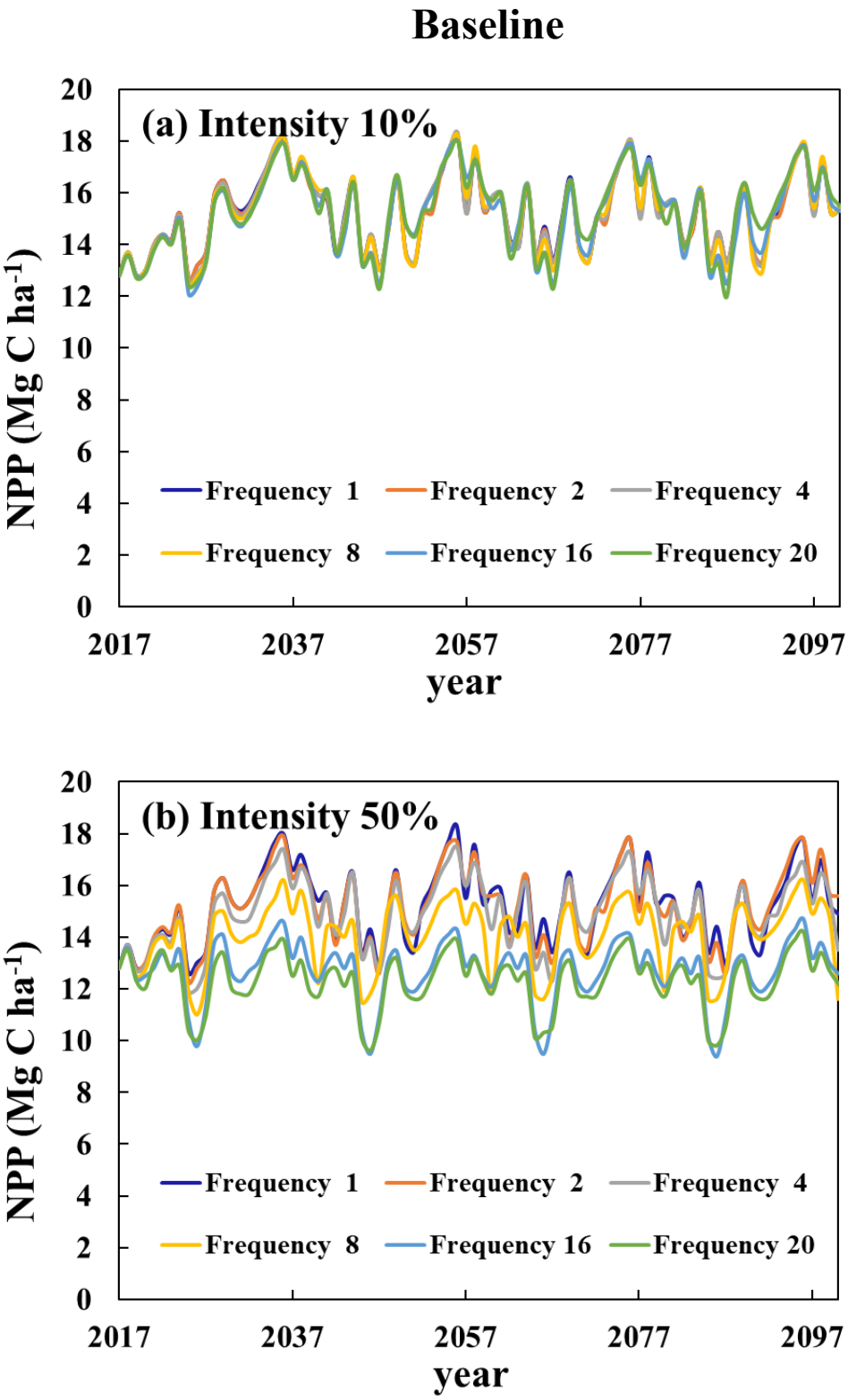


Figure 24. Net primary production (NPP) simulated in the baseline scenario. Time series of NPP from 2017 to 2100 in the case of typhoon intensity of (a) 10% and (b) 50%.

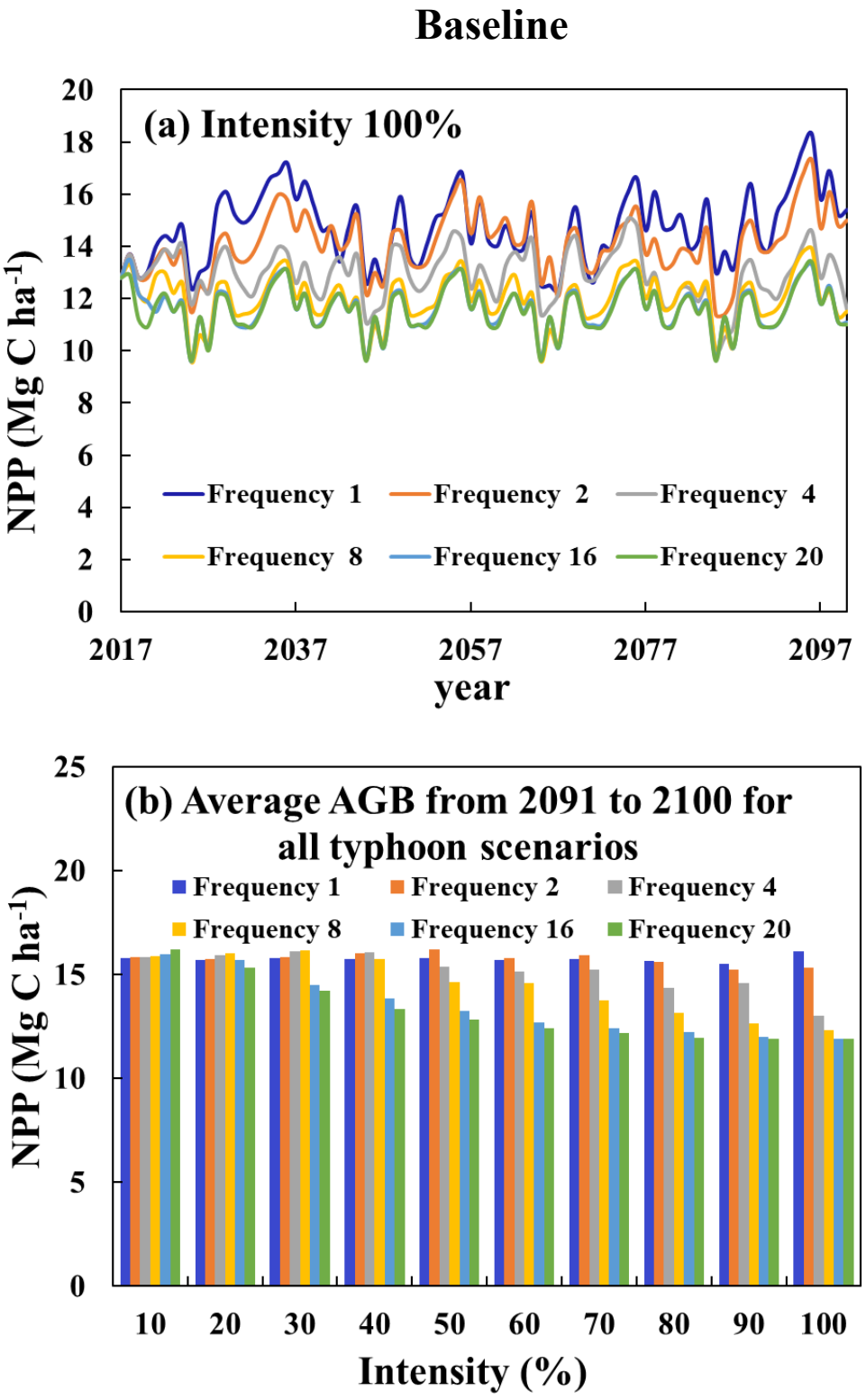


Figure 25. Net primary production (NPP) simulated in the baseline scenario: time series of NPP from 2017 to 2100 in the case of typhoon intensity of (a) 100% and (b) average NPP in the last decade (2091–2100) for different typhoon scenarios.

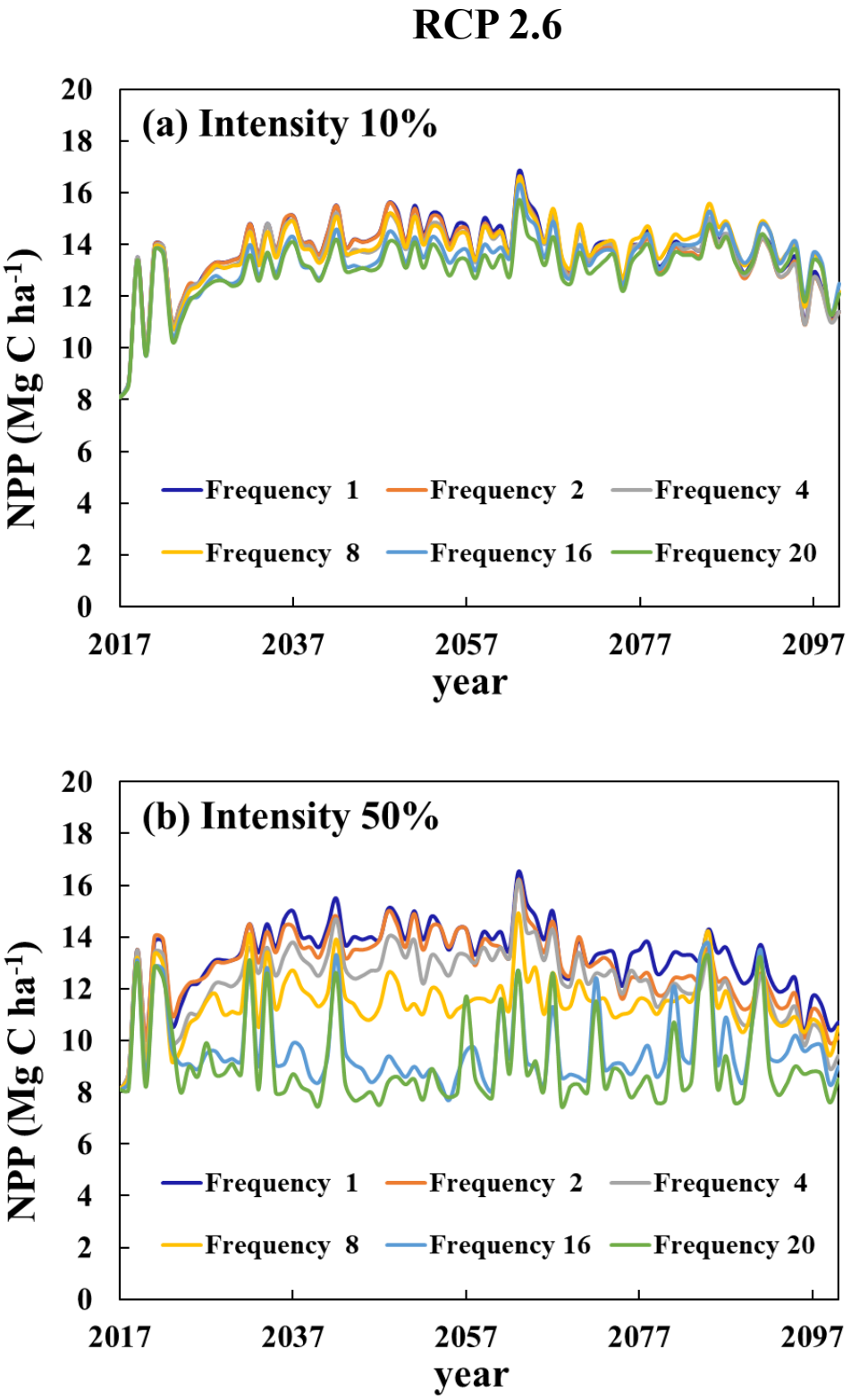


Figure 26. Net primary production (NPP) simulated in the RCP 2.6 scenario. Time series of NPP from 2017 to 2100 in the case of typhoon intensity of (a) 10% and (b) 50%.

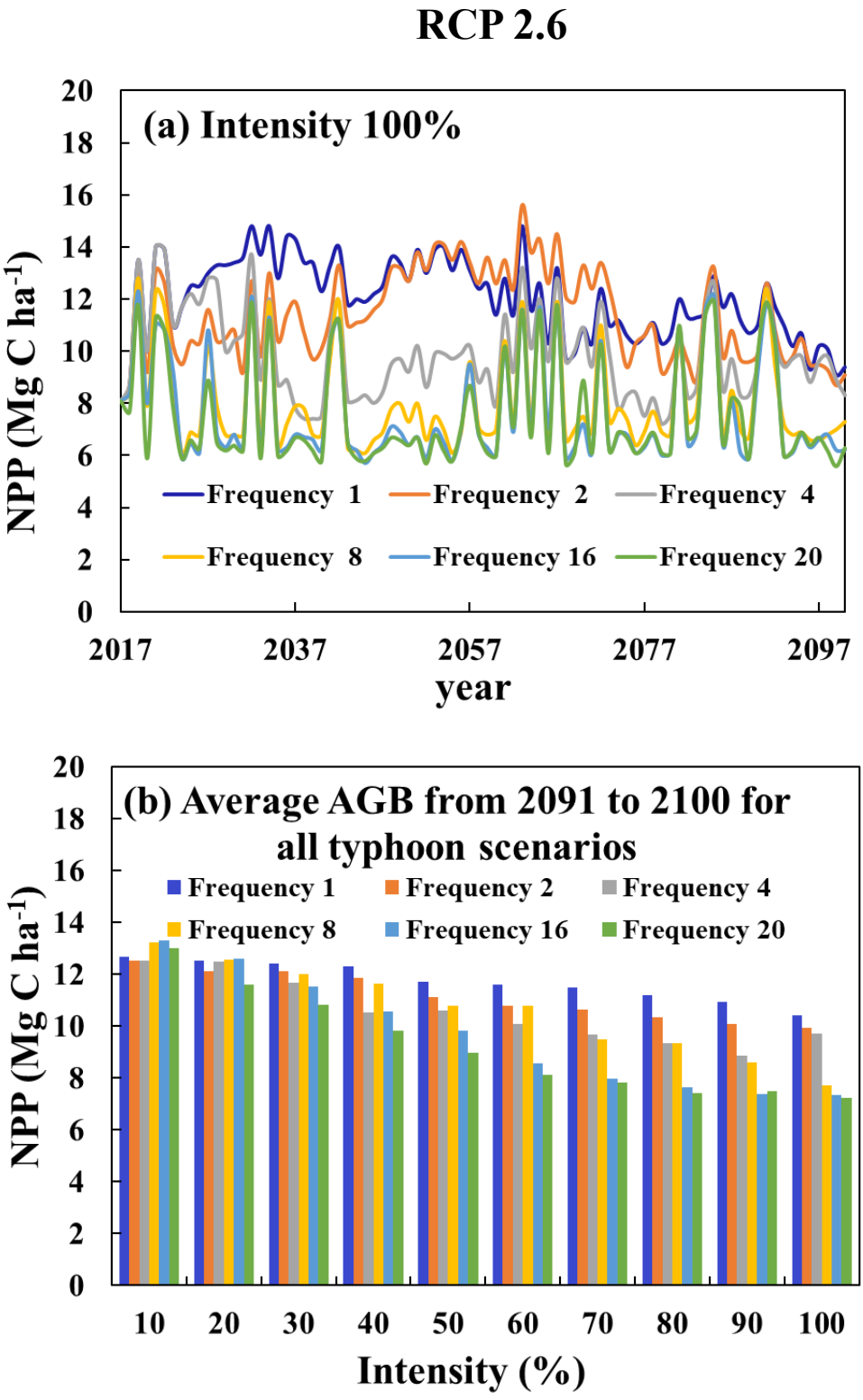


Figure 27. Net primary production (NPP) simulated in the RCP 2.6 scenario: time series of NPP from 2017 to 2100 in the case of typhoon intensity of (a) 100% and (b) average NPP in the last decade (2091–2100) for different typhoon scenarios.

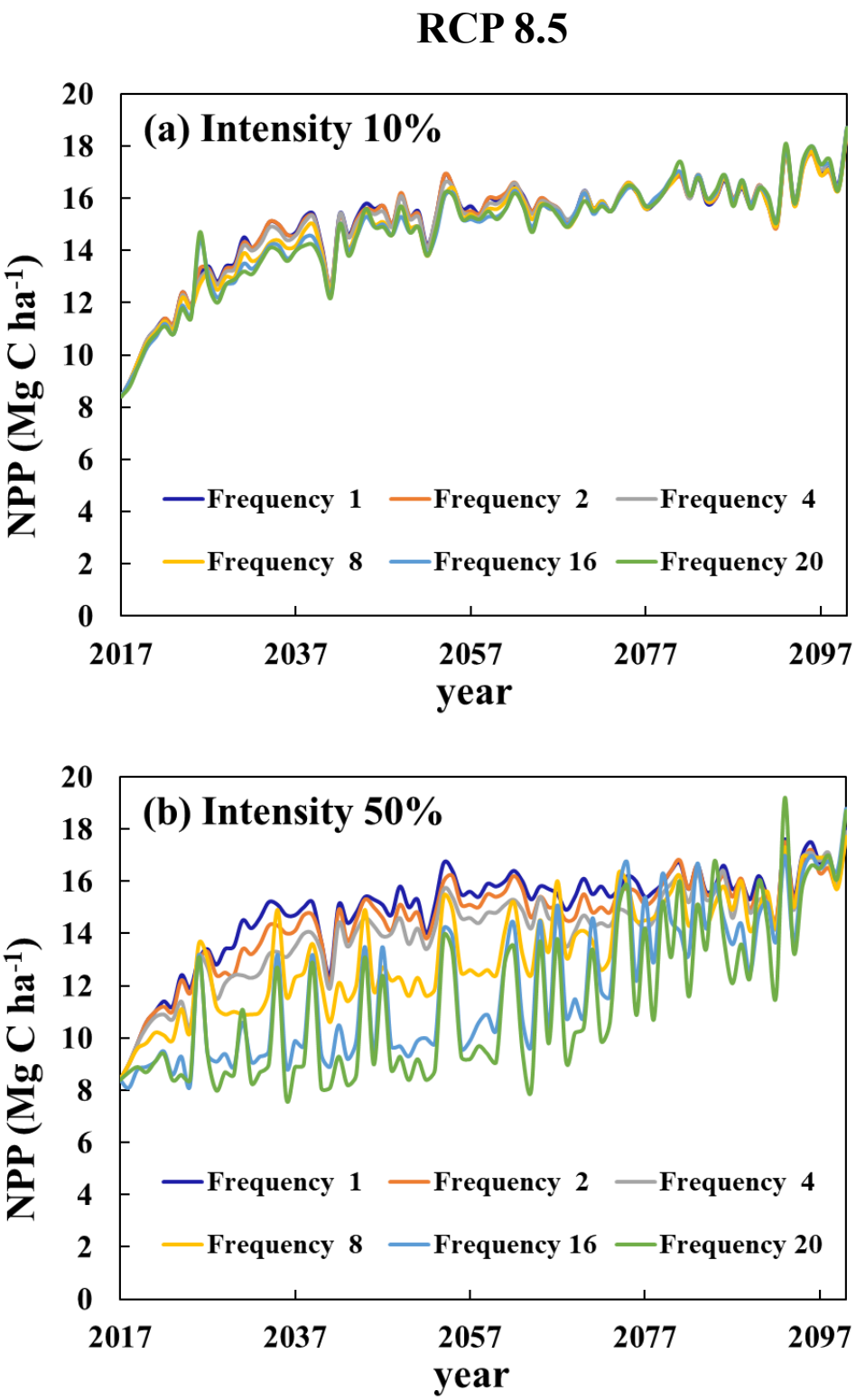


Figure 28. Net primary production (NPP) simulated in the RCP 2.6 scenario. Time series of NPP from 2017 to 2100 in the case of typhoon intensity of (a) 10% and (b) 50%.

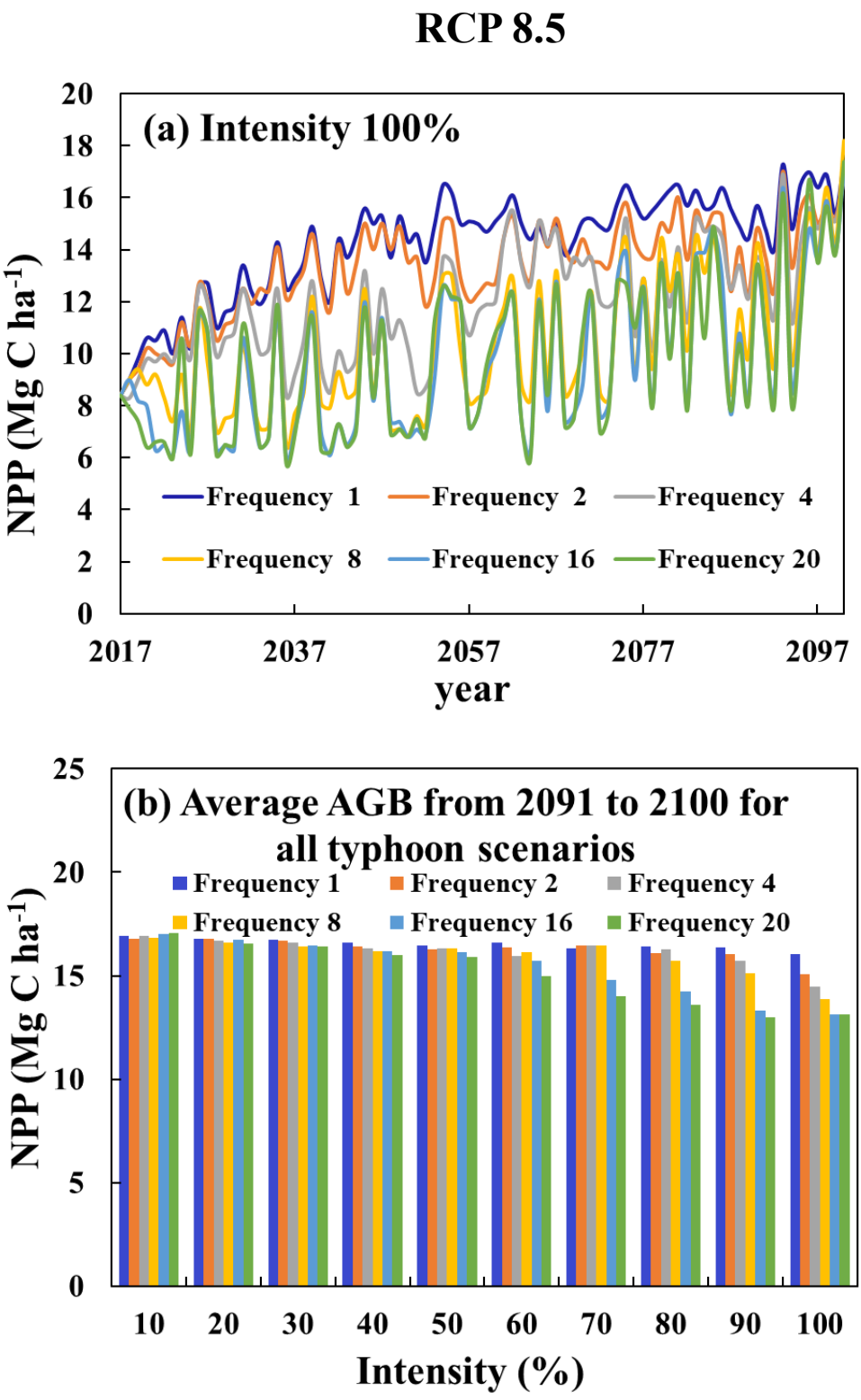


Figure 29. Net primary production (NPP) simulated in the RCP 8.5 scenario: time series of NPP from 2017 to 2100 in the case of typhoon intensity of (a) 100% and (b) average NPP in the last decade (2091–2100) for different typhoon scenarios.

IV. Discussion

IV-1. Representativeness of forest and carbon dynamics in the past and present after two typhoons

SEIB-DGVM properly reconstructed the interannual variations in forest dynamics and carbon cycle (Figs. 9-11). However, there are also some uncertainties included in the representativeness of forest and carbon dynamics after typhoon from the localization of model. The GPP and RE before the typhoon in 2004 were both overestimated, and the GPP after the typhoon was slightly overestimated. The slope of simulated GPP after the typhoon (Fig. 10 a) was systematically lower than the slope of values before the typhoon (Fig. 9 a), indicating that the effect of the typhoon on GPP was overestimated. Similarly, the effect of the typhoon on forest RE was overestimated. However, the slope of the ratio of simulated GPP to observed GPP from before to after the typhoon was 1.38 and that of RE was 1.32, indicating the effect of the typhoon on NEP would not be overestimated very much. AGB and LAI after the typhoon in 2004 were both underestimated, which may have arisen due to the random selection of tree mortality. Yoshida et al. (2009) investigated tree vulnerability to strong winds in northern Japan after the typhoon in 1954. They found that tree species with a high crown depth/height were more easily uprooted. In tropical dry forest, Jimenez-Rodríguez et al. (2018) found the most severe damage tended to occur to taller trees. Therefore, the random selection of trees performed in this study may differ from real forest damage, resulting in slight underestimation of the model results.

After the typhoon in 2004, the broad-leaved trees grew more quickly than the needle-leaved trees and consequently the broad-leaved species became dominant by 2012 at the Tomakomai Flux Research Site. Our simulation results agreed quantitatively with a biometric study showing that birch (*B. platyphylla and B. ermanii*) accounted for 51% of

the total population and 78% of the total biomass of overstory deciduous trees in 2014 (Yazaki et al., 2016).

Our results showed that NEP dramatically decreased around 1954, 1984, and 2004 (Fig. 12 a). There were three sharp shifts from carbon sink to source after 1954, 1984, and 2004, and the forest then gradually returned to a carbon sink over several years. Hirata et al. (2014), who used VISIT (Vegetation Integrative Simulator for Trace gases) to simulate the forest at the Tomakomai Flux Research Site, noted a similar trend. The trees damaged by typhoon Toyamaru in 1954 were clear-cut, and then Japanese larch was planted. The decline in NEP after 1954 reflected the conversion from mixed forest to larch plantation, and the NEP decline in 2004 was also due to a typhoon disturbance. The decrease in NEP in 1984, which resulted from much lower precipitation (694 mm) than normal (1000 mm), was far less than the two declines due to typhoon disturbance.

Our result showed that by 2017 the values of GPP and NPP had recovered to those prior to the typhoon (Fig. 12 a), but tree height, DBH, and AGB were still lower (Fig. 12 b, Fig. 30). The core reason is that height and DBH reflect the accumulation of biomass over multiple years, whereas NPP and GPP represent carbon flux, reflecting the ability of forest to absorb atmospheric carbon. At 14 y after the typhoon, the forest was still recovering slowly (Fig. 4). In addition, after the old trees in the forest were blown down by the typhoon, the productivity of new trees would be stronger than before. However, since the total structure of the ecosystem was not yet restored (e.g., LAI, DBH), the overall NPP and GPP were consistent with the previous situation.

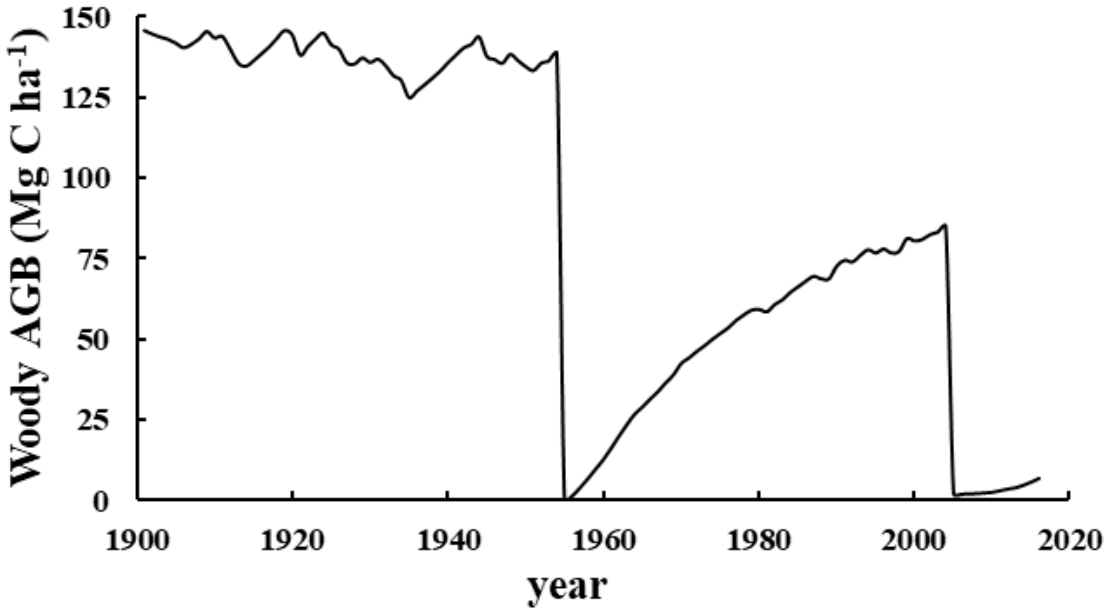


Figure 30. Time series of Woody AGB from 1901 to 2017

Ⅳ-2. Effect of typhoon disturbance on forest dynamics in the future

Our sensitivity analysis indicates that increasing typhoon frequency and intensity will result in a great decline in AGB and thus forest production. Previous simulation studies also found that increasing typhoon frequency results in lower forest AGB (Boose et al., 2004, Holm et al., 2017). A field experiment in a subtropical rainforest in Fushan, China, revealed that increasing typhoon frequency changed the structure and function of the forest ecosystem, with regard to carbon sequestration, carbon stock, and forest stature (Lin et al., 2017). Our simulations indicate that if typhoon frequency is $\leq$ 2 and intensity is $\leq$ 40%, AGB can recover to that before typhoon Songda by the end of the 21st century (Fig. 13-18). In a sensitivity simulation reported by O’ Brien et al. (1992), they simulated hurricane frequency and intensity by increasing the number of hurricanes from zero to one per year and tree mortality from 0% to 100%. They found that increasing hurricane strength decreased forest structural traits (basal area, biomass, and LAI) more than noted in our simulation of the Tomakomai site. Ground-based measurements also confirmed that tropical forest on the Pacific coast of Mexico had a lower tree height after a high-intensity hurricane in 2015 than before the storm (Jimenez-Rodríguez et al., 2018), and a semi-deciduous dry forest on the southwestern coast of Puerto Rico showed an overall reduced forest height due to frequent hurricane strikes (Van Bloem et al., 2007). In our simulation, the forest would no longer exist in the case of extremely high frequency and intensity (Fig. 19 a and b; Fig. 20 b), because tree regrowth would be interrupted so frequently and intensely that the forest could not accumulate enough biomass in the short typhoon return interval. Thus, our study shows very similar responses of AGB, tree height, and LAI to increasing storm strength as reported previously.

Our results also showed that AGB is higher under RCP 8.5 than RCP 2.6 and baseline. The RCP 2.6 and RCP 8.5 scenarios are defined such that the radiative forcing pathway increases to 2.6 and 8.5 W m^{-2} in 2100 (Van Vuuren et al., 2011). RCP 8.5 leads to higher CO_2 concentration levels than RCP 2.6. Because CO_2 is a greenhouse gas, increasing the CO_2 concentration will cause an increase in temperature. The temperature of the Tomakomai site will increase by 1.3 °C (RCP 2.6) and 5.2 °C (RCP 8.5) from 2017 to 2100, and the CO_2 concentration will increase by 16 ppm (RCP 2.6) and 529 ppm (RCP 8.5) in the same period. Increasing the CO_2 concentration in the atmosphere will enhance the photosynthesis rate and thus greater productivity will be achieved. The elevated temperature can also extend the vegetation growing season. The higher value of AGB under RCP 8.5 compared to RCP 2.6 was the result of higher gross and net productivity. Achat et al. (2018) also reported that the harvested biomass is much greater under RCP8.5 compared to RCP 2.6. When a typhoon occurs only once in the simulation period, however, AGB shows a slight increase when intensity is 100% under RCP 8.5 (Fig. 18 b). One possible explanation for this result is that there is some bias when typhoon frequency is 1. Again, the year in which the typhoon occurred was randomly selected (Appendix 8) by dividing the future period into several parts according to the typhoon frequency. To reduce this bias, the simulations were repeated 10 times for each group of typhoon scenarios, but there may still have been some uncertainty at lower frequency. When the randomly selected typhoon years were concentrated in the first half of the 21st century, due to the early arrival of the typhoon, the trees had already recovered by the end of the 21st century.

In contrast, understory grass LAI increases along with typhoon strength, mainly as a result of increased light intensity reaching the ground. Frequent typhoons result in frequent windthrow and large and regularly existing canopy gaps (Yao et al., 2015). Understory plants can receive more light, which increases their growth rate, thus leading to a higher grass LAI (Fig. 20 a).

To quantify the storm impact, linear regression functions was presented expressing the relationships between forest traits (AGB, tree height, tree density, woody LAI, and grass LAI) and typhoon frequency or intensity under the RCP2.6 and RCP8.5 scenarios. The equation for AGB under RCP2.6 (Eq. 7) and RCP8.5 (Eq. 8) is as follow (±95% confidence interval):

Under RCP2.6,

$$AGB_{2100} = 125.39\ (\pm 12.89) - 3.54\ (\pm 1.16)\ F - 0.93\ (\pm 0.21)\ I - 0.01\ (\pm 0.02)\ F \times I \quad (7)$$

and under RCP8.5,

$$AGB_{2100} = 133.60\ (\pm 13.23) - 3.15\ (\pm 1.19)\ F - 0.76\ (\pm 0.21)\ I - 0.01\ (\pm 0.02)\ F \times I, \quad (8)$$

where AGB_{2100} is the average AGB in the last decade of the simulation (2091–2100; Mg C ha^{-1}), F is the typhoon frequency (times per 84 y), and I is the typhoon intensity (%). The residuals are small and R^2 values are relatively high (0.84 and 0.85 for RCP2.6

and RCP8.5, respectively). Thus, these two equations can be used to predict the AGB loss with increasing frequency and intensity of typhoon under RCP2.6 and RCP8.5.

The equation for tree height (m) under RCP2.6 (Eq. 9) and RCP8.5 (Eq. 10) is as follow (±95% confidence interval):

Under RCP2.6,

$$\text{tree height}_{2100} = 7.23\ (\pm 0.41) + 0.04\ (\pm 0.04)\ F + 0.0004\ (\pm 0.01)\ I - 0.003\ (\pm 0.0006)\ F \times I, \quad (9)$$

and under RCP8.5,

$$\text{tree height}_{2100} = 5.72\ (\pm 0.15) + 0.01\ (\pm 0.01)\ F - 0.01\ (\pm 0.003)\ I - 0.002\ (\pm 0.0002)\ F \times I, \quad (10)$$

where $\text{tree height}_{2100}$ is the average of tree height in the last decade of the simulation (2091–2100; m), F is the typhoon frequency (times per 84 y), and I is the typhoon intensity (%). The residuals are small and R^2 values are relatively high (0.89 and 0.96 for RCP2.6 and RCP8.5, respectively). Thus, these two equations can be used to predict the tree height under RCP2.6 and RCP8.5.

The equation for tree density (trees ha^{-1}) under RCP2.6 (Eq. 11) and RCP8.5 (Eq. 12) is as follow (±95% confidence interval):

Under RCP2.6,

$$\text{tree density}_{2100} = 1597\ (\pm 86) - 33.12\ (\pm 7.78)\ F - 4.50\ (\pm 1.39)\ I - 0.02\ (\pm 0.12)\ F \times I, \quad (11)$$

and under RCP8.5,

$$\text{tree density}_{2100} = 2718\ (\pm 150.11) - 39.72\ (\pm 13.51)\ F - 4.67\ (\pm 2.42)\ I - 0.45\ (\pm 0.22)\ F \times I, \quad (12)$$

where tree density$_{2100}$ is the average tree density in the last decade of the simulation (2091–2100), F is the typhoon frequency (times per 84 y), and I is the typhoon intensity (%). The residuals are small and R^2 values are relatively high (0.9 and 0.91 for RCP2.6 and RCP8.5, respectively). Thus, these two equations can be used to predict the tree density under RCP2.6 and RCP8.5.

The equation for woody LAI ($m^2\ m^{-2}$) under RCP2.6 (Eq. 13) and RCP8.5 (Eq. 14) is as follow (±95% confidence interval):

Under RCP2.6,

$$\text{woody LAI}_{2100} = 4.08\ (\pm 0.36) - 0.04\ (\pm 0.03)\ F - 0.02\ (\pm 0.01)\ I - 0.001\ (\pm 0.0005)\ F \times I, \quad (13)$$

and under RCP8.5,

$$\text{woody LAI}_{2100} = 5.59\ (\pm 0.34) - 0.02\ (\pm 0.03)\ F - 0.01\ (\pm 0.01)\ I - 0.003\ (\pm 0.0005)\ F \times I, \quad (14)$$

where woody LAI_{2100} is the average woody LAI in the last decade of the simulation (2091–2100), F is the typhoon frequency (times per 84 y), and I is the typhoon intensity (%). The residuals are small and R^2 values are relatively high (0.89 and 0.95 for RCP2.6 and RCP8.5, respectively). Thus, these two equations can be used to predict the woody LAI under RCP2.6 and RCP8.5.

The equation for grass LAI (m^2 m^{-2}) under RCP2.6 (Eq. 15) and RCP8.5 (Eq. 16) is as follow (±95% confidence interval):

Under RCP2.6,

$$\text{grass } LAI_{2100} = 0.57\ (\pm 0.18) + 0.02\ (\pm 0.02)\ F + 0.01\ (\pm 0.003)\ I + 0.0001\ (\pm 0.0003)\ F \times I, \quad (15)$$

and under RCP8.5,

$$\text{grass } LAI_{2100} = 1.05\ (\pm 0.22) + 0.01\ (\pm 0.02)\ F + 0.01\ (\pm 0.004)\ I + 0.002\ (\pm 0.0003)\ F \times I, \quad (16)$$

where grass LAI_{2100} is the average grass LAI in the last decade of the simulation (2091–2100), F is the typhoon frequency (times per 84 y), and I is the typhoon intensity (%). The residuals are small and R^2 values are relatively high (0.92 and 0.96 for RCP2.6 and RCP8.5, respectively). Thus, these two equations can be used to predict the grass LAI under RCP2.6 and RCP8.5.

Ⅳ-3. Effect of typhoon disturbance on carbon dynamics in the future

NPP, a key component of the terrestrial carbon cycle, is defined as the balance between carbon gain by photosynthesis and carbon loss by autotrophic respiration. NPP tends to decrease after a disturbance due to loss of LAI and then gradually increases over time until the canopy closes (Chapin et al., 2002). Thus, the NPP rate during the last 10 years of the simulation period depends on the frequency and intensity of storms, as well as on climatic factors determining the potential NPP rate, especially in the future. In our simulations, NPP in the last decade decreased significantly by increasing typhoon intensity but not by increasing typhoon frequency (Fig. 22 a). In contrast, Holm et al. (2017) reported that in a tropical forest (Luquillo Experimental Forest, Puerto Rico) NPP increased in response to increasing hurricane frequency but not to increasing intensity. A possible mechanism to explain this difference is that the recovery of forest LAI, as the basis of photosynthesis, proceeds very slowly in the Tomakomai forest due to the cool climate, whereas it occurs very quickly in the tropical forest due to the warm climate. Moreover, there were also differences in model structure and parameterization. Our model is tuned for the Tomakomai forest, which is exposed to much less frequent but more destructive storm events (typhoons Toyamaru in 1954 and Songda in 2004), whereas that of Holm et al. (2017) is tuned to forest on Puerto Rico, which is exposed to more frequent hurricanes that damage leaves and branches every 4 years, blow down trees and make small gaps every 6 y, and cause extensive blowdowns every 15–30 years (Boose et al., 2004). The lower typhoon frequency in Tomakomai leads to higher forest density, and the high-density forest is vulnerable to typhoons of greater intensity due to the relatively

weak roots. Therefore, the decline in NPP was more strongly affected by typhoon intensity in our study.

After a disturbance, the forest can gradually regenerate. When the disturbance occurs frequently and periodically, the forest will be forced to adapt to the new environmental conditions. Some tree species that cannot regrow quickly will gradually be reduced, and new species that can adapt to the new environment will become the dominant species. In regions with high typhoon frequency and low typhoon intensity, the dominant species can adapt to the strong wind. Because typhoons mainly damage the branches and leaves, the increasing frequency will cause more woody debris and litter, thus having a greater impact on NPP and HR. In regions with low-frequency and high-intensity typhoons, the forest is very vulnerable to strong wind. The main typhoon damages are stem breakage and uprooting of trees. Thus, the increasing intensity will result in more biomass loss, which will have a greater impact on NPP.

Our results also showed that increasing typhoon frequency and intensity had a greater influence on AGB than NPP. After a typhoon disturbance, more light reaches the forest floor due to the formation of canopy gaps (Fig. 32). Consequently, photosynthesis of the grass increases rapidly, and grass NPP can recover quickly. The recovery of woody AGB after each typhoon event requires more time than the recovery of NPP. In this study, the highest typhoon frequency was, on average, every 4.2 years (20 times from 2017 to 2100). NPP can be recovered in 4.2 years, but AGB will take longer to recover.

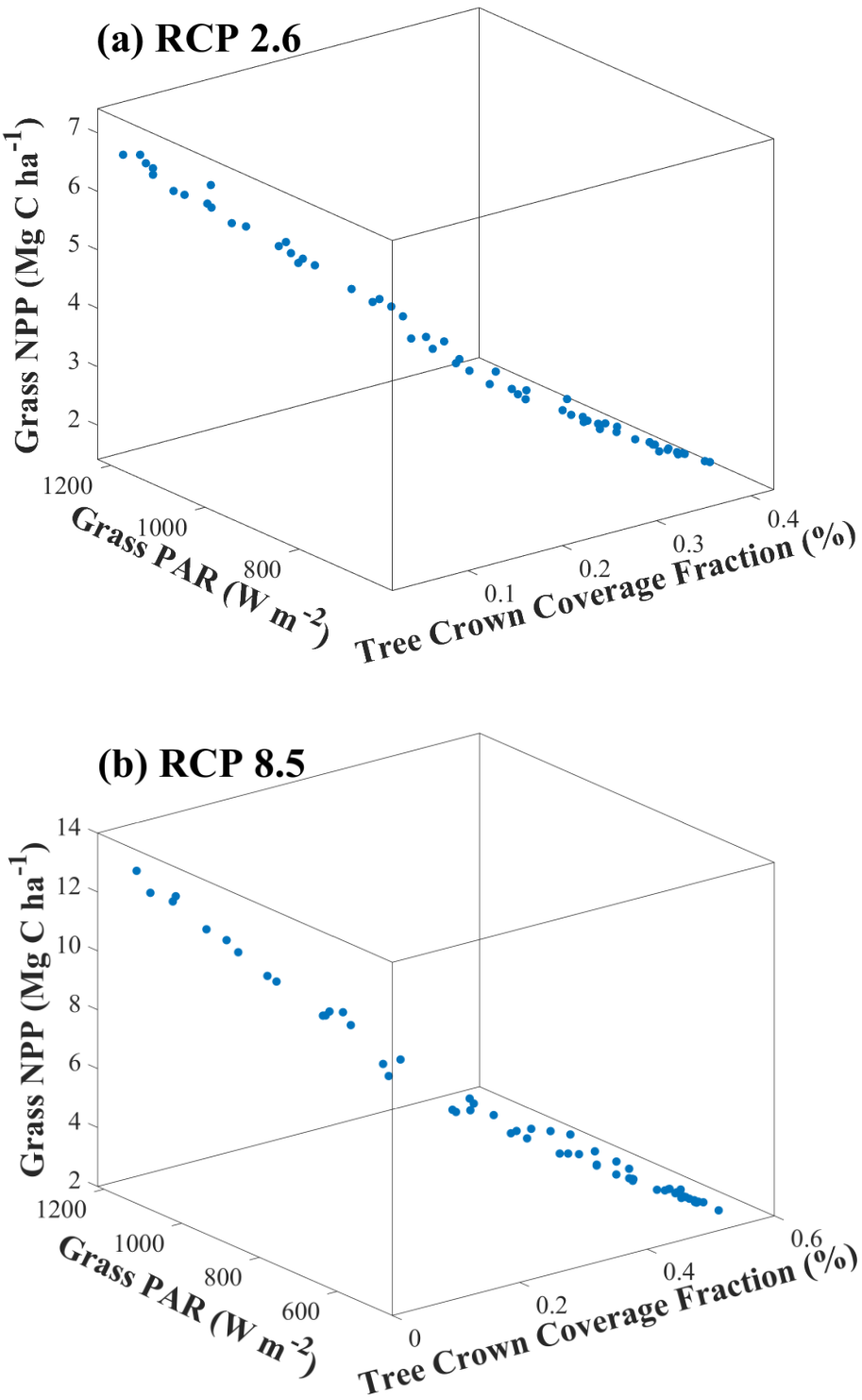


Figure 32. Three-dimensional scatter plot of grass NPP, grass PAR, and tree crown coverage fraction under (a) RCP2.6 and (b) RCP8.5 scenarios. Values are average for the last decade of the 21st century (2091–2100).

Finally, the linear functions were calculated between carbon balance and typhoon frequency and intensity under the RCP2.6 and RCP8.5 scenarios. The equation for NPP (Mg C ha^{-1} y^{-1}) under RCP2.6 (Eq. 17) and RCP8.5 (Eq. 18) is as follow (±95% confidence interval):

Under RCP2.6,

$$NPP_{2100} = 13.06\ (\pm 0.45) + 0.01\ (\pm 0.04)\ F - 0.03\ (\pm 0.01)\ I - 0.002\ (\pm 0.0006)\ F \times I, \quad (17)$$

and under RCP8.5,

$$NPP_{2100} = 16.96\ (\pm 0.30) + 0.05\ (\pm 0.03)\ F - 0.01\ (\pm 0.01)\ I - 0.002\ (\pm 0.0004)\ F \times I, \quad (18)$$

where NPP_{2100} is the average NPP in the last decade (2091–2100), F is the typhoon frequency (times per 84 y), and I is the typhoon intensity (%). With relatively high R^2 values (0.85 and 0.73 for RCP2.6 and RCP8.5, respectively), these two equations appear to be able to predict the NPP gain with increasing typhoon frequency and intensity.

The equation for HR (Mg C ha^{-1} y^{-1}) under RCP2.6 (Eq. 19) and RCP8.5 (Eq. 20) is as follow (±95% confidence interval):

Under RCP2.6,

$$HR_{2100} = 14.14\ (\pm 0.65) - 0.25\ (\pm 0.06)\ F - 0.06\ (\pm 0.01)\ I + 0.001\ (\pm 0.0009)\ F \times I, \quad (19)$$

and under RCP8.5,

$$HR_{2100} = 17.46\ (\pm 0.90) - 0.28\ (\pm 0.08)\ F - 0.06\ (\pm 0.01)\ I + 0.002\ (\pm 0.001)\ F \times I, \quad (20)$$

where HR2100 is the average heterotrophic respiration in the last decade of the simulation (2091–2100), F is the typhoon frequency (times per 84 y), and I is the typhoon intensity (%). The residuals are small and R^2 values are relatively high (0.87 and 0.76 for RCP2.6 and RCP8.5, respectively). Thus, these two equations can be used to predict the HR under RCP2.6 and RCP8.5.

In our simulation, as typhoon frequency and intensity increase, the NEP, a net carbon flux, first increases and then decreases (Fig. 22 b). As the typhoon frequency and intensity increase, heterotrophic respiration first decreases quickly and then remains stable (Fig. 23), whereas NPP first remains stable and then decreased quickly. Therefore, the difference between NPP and heterotrophic respiration first increases and then decreases as typhoon frequency and intensity increase. Increasing the typhoon frequency and intensity had a greater influence on heterotrophic respiration than NPP. Therefore, the results predict that the forest will become a carbon sink under different typhoon scenarios at the end of the 21st century. Ito (2010) estimated the loss of forest carbon gain of nearly 200 g C m^{-2} y^{-1} after 10 typhoons struck Japan in 2004, as large storm disturbance enhances tree mortality and causes a large reduction in carbon uptake (Amiro et al., 2010, Barr et al., 2010). On the other hand, there is sometimes no significant effect on NEE when a smaller disturbance occurs, especially at a lower frequency (Li et al., 2007, Powell et al., 2008). Therefore, there is no common observed trend for the NEE after typhoon disturbances.

Ⅳ-4. Limitations

In this study, typhoon intensity was represented by tree mortality. A certain percentage of trees was killed randomly depending on the typhoon intensity. However, wind direction, wind speed, forest structure, site conditions, and tree characteristics are all important factors that influence the susceptibility of trees to wind damage. By incorporating a wind damage risk model (e.g., ForestGALES) in SEIB-DGVM, the simulation of tree damage by wind may be closer to reality. In addition, typhoon year was randomly selected as well. When the typhoon frequency is 1, there is still some bias under RCP8.5.

V. Summary

The impact of disturbance on the main ecological processes of forest ecosystems and the response of forest ecosystem to disturbances have become an international frontiers and hotspots in the field of forest ecology research. Therefore, it has important scientific and practical significance to study the disturbed ecosystem. In this study, an individual-based dynamic vegetation model was used to investigate how typhoon disturbance in the future may impact cool temperature forests, with a local forest in Tomakomai Flux research site in northern Japan. This study investigated the effects of typhoon frequency and intensity on forest structure, carbon stocks and recovery and tested the sensitivity of vegetation status to the future climate.

There are two main objectives in this study: (1) reproducing the forest structural traits and carbon dynamics in Tomakomai in the historical period by using SEIB-DGVM; and (2) evaluating the possible impact of typhoons on the forest under projected future climate changes. GPP and RE before and after typhoon Songda in 2004 was validated. AGB and LAI after typhoon also shows a high correlation coefficient. Therefore, SEIB-DGVM can reproduced the observed interannual variations at the Tomakomai Flux Research Site before and after typhoon Songda and it is considered that it can be used in the prediction of the future period.

In the future period simulation, our results suggest that increasing typhoon frequency and intensity have a significant effect on forest and carbon dynamics under both RCP2.6 and RCP8.5. As the frequency and intensity of typhoons increase, AGB and NPP decrease. However, increasing typhoon frequency and intensity had a greater influence on AGB than NPP. The values of AGB and NPP are much higher under RCP8.5 as compared to those under RCP2.6 and baseline. As the frequency and intensity of typhoons increase,

NEP first increases and then decreases. Our simulations indicate that the forest at the Tomakomai site will become a carbon sink under different typhoon scenarios at the end of the 21st century. In addition, our analysis indicates that if typhoon frequency were $\leq$ 2 and intensity were $\leq$ 40% in the future (under RCP2.6 and RCP8.5), forest AGB can recover to that before typhoon Songda by the end of the 21st century. Furthermore, the result shows strong linear relationships between forest traits (AGB, tree height, tree density, and woody and grass LAI) and carbon dynamics (NPP, NEP) with typhoon frequency and intensity, respectively. These regression equations can be used not only by researchers, but also by stakeholders, to account for predicted carbon gain in the future.

VI. References

Achat, D. L., Martel, S., Picart, D., Moisy, C., Augusto, L., Bakker, M. R., Loustau, D., 2018. Modelling the nutrient cost of biomass harvesting under different silvicultural and climate scenarios in production forests. For. Ecol. Manag., 429, 642–653.

Amiro, B.D., Barr, A.G., Barr, J.G., Black, T.A., Bracho, R., Brown, M., Chen, J., Clark, K.L., Davis, K.J., Desai, A.R., et al., 2010. Ecosystem carbon dioxide fluxes after disturbance in forests of North America, J. Geophys. Res. 115, G00K02, doi: 10.1029/2010JG001390.

Ancelin, P., Courbaud, B., Fourcaud, T., 2004. Development of an individual tree-based mechanical model to predict wind damage within forest stands. For. Ecol. Manag. 203, 101–121, doi: 10.1016/j.foreco.2004.07.067.

Ball, J. T., Woodrow, I. E., & Berry, J. A., 1987. A model predicting stomatal conductance and its contribution to the control of photosynthesis under different environmental conditions. In Progress in photosynthesis research (pp. 221-224). Springer, Dordrecht.

Barr, J.G., Engel, V., Fuentes, J.D., Zieman, J.C., O'Halloran, T.L., Smith III, T.J., Anderson, G.H., 2010. Controls on mangrove forest-atmosphere carbon dioxide exchanges in western Everglades National Park, J. Geophys. Res. 115, G02020, doi:10.1029/2009jg001186.

Boose, E.R., Serrano, M.I., Foster, D.R., 2004. Landscape and regional impacts of hurricanes in Puerto Rico. Ecol. Mono. 74, 335–352.

Botta, A., Viovy, N., Ciais, P., Friedlingstein, P., & Monfray, P., 2000. A global prognostic scheme of leaf onset using satellite data. Global Change Biology, 6(7), 709-725.

Chambers, J.Q., J.I. Fisher, H.C. Zeng, E.L. Chapman, D.B. Baker, G.C. Hurtt, 2007. Hurricane Katrina's carbon footprint on U.S. Gulf Coast forests, Science, 318, 1107,

doi:10.1126/science.1148913.

Chapin, F.S., Ⅲ, Matson PA, Mooney H A., 2002. Principles of Terrestrial Ecosystem Ecology. Springer, New York.

Chapman, E.L., et al., 2008. Hurricane Katrina impacts on forest trees of Louisiana's Pearl River basin. For. Ecol. Manag. 256, 883–889, doi.org/10.1016/j.foreco.2008.05.057.

Chen, H., Lu, W., Yan, G., Yang, S., Lin, G., 2014. Typhoons exert significant but differential impacts on net ecosystem carbon exchange of subtropical mangrove forests in China. Biogeosciences 11, 5323–5333, doi:10.5194/bg-11-5323-2014.

Chen, S., Komiyama, A., Kato, S., Cao, R., Yoshitake, S., Ohtsuka, T., 2017. Stand dynamics and biomass increment in a lucidophyllous forest over a 28-year period in central Japan. Forests 8, 1–14, doi:10.3390/f8100397.

Chen, Y. et al., 2017. Simulating damage for wind storms in the land surface model ORCHIDEE-CAN (revision 4262). Geosci. Model Dev. Discuss. 174, 1–34, doi:10.5194/gmd-2017-174.

Chi, C.H. et al., 2015. Typhoon disturbance mediates elevational patterns of forest structure, but not species diversity, in humid monsoon Asia. Ecosystems 18, 1410–1423, doi: 10.1007/s10021-015-9908-3.

Cooper-Ellis, S., Foster, D.R., Carlton, G., Lezberg, A., 1999. Forest response to catastrophic wind: results from an experimental hurricane. Ecology 80, 2683–2696.

Cramer, W., Bondeau, A, Woodward, FI, Prentice, IC, Betts, RA, et al., 2001. Global response of terrestrial ecosystem structure and function to CO2 and climate change: results from six dynamic global vegetation models. Glob. Change Biol. 7, 357–373.

Emori, S., A. Hasegawa, T. Suzuki, and K. Dairaku, 2005. Validation, parameterization

dependence, and future projection of daily precipitation simulated with a high-resolution atmospheric GCM, Geophys. Res. Lett. 32, L06708, doi:10.1029/2004GL022306.

Field, C.B., et al., 2012. Managing the risks of extreme events and disasters to advance climate change adaptation. Cambridge University Press, Cambridge, UK.

Fisher, R. A., Koven, C. D., Anderegg, W. R. L., Christoffersen, B. O., Dietze, M. C., Farrior, C., … Moorcroft, P., 2018. Vegetation demographics in Earth system models: a review of progress and priorities. Global Change Biology, 24, 35–54.

Foley, J. A., 1995. An equilibrium model of the terrestrial carbon budget. Tellus B: Chemical and Physical Meteorology, 47(3), 310-319.

Foster, D.R., 1988. Species and stand response to catastrophic wind in central New England, USA. Journal of Ecology, 76, 135–151.

Fujii, S., Kubota, Y., & Enoki, T. , 2009. Resilience of stand structure and tree species diversity in subtropical forest degraded by clear logging. Journal of forest research, 14(6), 373-387.

Gardiner, B., Peltola, H. and Kellomaki, S., 2000. Comparison of two models for predicting the critical wind speeds required to damage coniferous trees. Ecol. Model. 129, 1–23.

Hajima, T., Ise, T., Tachiiri, K., Kato, E., Watanabe, S., Kawamiya, M., 2012. Climate change, allowable emission, and Earth system response to representative concentration pathway scenarios, J. Meteor. Soc. Japan, 90, 417–433, doi: 10.2151/jmsj.2012-305.

Harris, I., P.D. Jones, T.J. Osborn, and D.H. Lister, 2014. Updated high-resolution grids of monthly climatic observations: the CRU TS3.10 Dataset, Int. J. Climatol., 34(3),

623–642, doi:10.1002/joc.3711.

Hirano, T., R. Hirata, Y. Fujinuma, N. Saigusa, S. Yamamoto, Y. Harazono,M. Takada, K. Inukai, and G. Inoue., 2003. CO2 and water vapor exchange of a larch forest in northern Japan, Tellus, Ser. B, 55, 244–257.

Hirano, T., Suzuki, K., Hirata, R., 2017. Energy balance and evapotranspiration changes in a larch forest caused by severe disturbance during an early secondary succession. Agric. For. Meteorol. 232, 457–468.

Hirata, R. et al., 2007. Seasonal and interannual variations in carbon dioxide exchange of a temperate larch forest. Agric. For. Meteorol. 147, 110–124, doi: 10.1016/j.agrformet.2007.07.005.

Hirata, R., Takagi, K., Ito, A., Hirano, T., Saigusa, N., 2014. The impact of climate variation and disturbances on the carbon balance of forests in Hokkaido, Japan. Biogeosciences 11, 5139–5154, doi:10.5194/bg-11-5139-2014.

Holm, J.A., Van Bloem, S.J., Larocque, G.R., Shugart, H., 2017. Shifts in biomass and productivity for a subtropical dry forest in response to simulated elevated hurricane disturbances. Environ. Res. Lett. 12, 1–13.

Huth, A., & Ditzer, T., 2000. Simulation of the growth of a lowland Dipterocarp rain forest with FORMIX3. Ecological Modelling, 134(1), 1-25.

Ide, R., Nakaji, T., Motohka, T., Oguma, H., 2011. Advantages of visible-band spectral remote sensing at both satellite and near-surface scales for monitoring the seasonal dynamics of GPP in a Japanese larch forest. J. Agric. Meteorol. 67, 75–84.

Ito, A., 2010. Evaluation of the impacts of defoliation by tropical cyclones on a Japanese forest's carbon budget using flux data and a process-based model. J. Geophys. Res., 115, G04013, doi:10.1029/2010JG001314.

Ito, A., Saigusa, N., Murayama, S., Yamamoto, S., 2005. Modeling of gross and net carbon dioxide exchange over a cool-temperate deciduous broad-leaved forest in Japan: Analysis of seasonal and interannual change, Agr. Forest Meteorol., 134, 122–134.

Jimenez-Rodríguez, D.L., Alvarez-Añorve, M.Y., Pineda-Cortes, M., et al., 2018. Structural and functional traits predict short term response of tropical dry forests to a high intensity hurricane [J]. Forest Ecology and Management, 426, 101–114.

K-1 Model Developers, 2004. K-1 Coupled GCM (MIROC) Description, K-1 Tech Rep. 1, edited by H. Hasumi and S. Emori, 39 pp., Center for Climate Systems Research, Univ. of Tokyo, Tokyo. [Available at www.ccsr.utokyo.ac.jp/kyosei/hasumi/MIROC/tech-repo.pdf.] (last access: 30 September 2011).

Kalnay, E., et al., 1996. The NCEP/NCAR 40-year reanalysis project, B. Am. Meteorol. Soc., 77(3), 437–471.

Kistler, R., Kalnay, E., Collins, W., Saha, S., White, G., Woollen, J., ... & van den Dool, H., 2001. The NCEP–NCAR 50-year reanalysis: monthly means CD-ROM and documentation. Bulletin of the American Meteorological society, 82(2), 247-268.

Knutson, T.R. et al., 2010. Tropical cyclones and climate change. Nat. Geosci. 3, 157–163, doi: 10.1038/NGEO779.

Leuning, R., 1995. A critical appraisal of a combined stomatal-photosynthesis model for C_3 plants. Plant, Cell & Environment, 18(4), 339-355.

Li, J., Powell, T. L., Seiler, T. J., Johnson, D. P., Anderson, H. P., Bracho, R., ... Drake, B. G., 2007. Impacts of Hurricane Frances on Florida scrub‐oak ecosystem processes: defoliation, net CO2 exchange and interactions with elevated CO2. Global Change

Biology, 13(6), 1101–1113.

Lin, K.C., et al., 2017. Impacts of increasing typhoons on the structure and function of a subtropical forest: reflections of a changing climate. Sci. Rep. 1–10, doi:10.1038/s41598-017-05288-y.

Lin, T.C. et al., 2011. Typhoon disturbance and forest dynamics: lessons from a Northwest Pacific subtropical forest. Ecosystems 14, 127–143, doi: 10.1007/s10021-010-9399-1.

Lloyd, J., & Taylor, J. A., 1994. On the temperature dependence of soil respiration. Functional ecology, 315-323.

Mei, W., Xie, S., 2016. Intensification of landfalling typhoons over the Northwest Pacific since the late 1970s. Nat. Geosci. 9, 753–757, doi: 10.1038/NGEO2792 Intensification.

Mei, W., Xie, S.P., Primeau, F., McWilliams, J.C., Pasquero, C., 2015. Northwestern Pacific typhoon intensity controlled by changes in ocean temperatures. Sci. Adv. 1, 1–8.

Monteith, J. L., & Unsworth, M. H., 1990. Principles of environmental physics Second edition. Edward Arnold, London.

Negrón-Juárez, R., Baker, D.B., Zeng, H., Henkel, T.K., Chambers, J. Q., 2010. Assessing hurricane-induced tree mortality in U.S. Gulf Coast forest ecosystems. J. Geophys. Res. Biogeosciences 115, 1–11.

O'Brien, ST, Hayden BP, Shugart HH., 1992. Global climatic change, hurricanes, and a tropical forest. Clim Change 22, 175–190.

Peltola, H., Kellomäki, S., Väisänen, H., Ikonen, V.P., 1999. A mechanistic model for assessing the risk of wind and snow damage to single trees and stands of Scots pine,

Norway spruce, and birch. Can. J. For. Res. 29, 647–661.

Peltola, H., Kellomäki, S., Hassinen, A., Granander, M., 2000. Mechanical stability of Scots pine, Norway spruce and birch: an analysis of tree-pulling experiments in Finland. For. Ecol. Manage. 135, 143–153.

Powell, T.L., Gholz, H.L., Clark, K.L., Starr, G., Cropper, W.P., Martin, T.A., 2008. Carbon exchange of a mature, naturally regenerated pine forest in north Florida, Glob. Change Biol., 14, 2523–2538, doi:10.1111/j.1365-2486.2008.01675.x.

Riahi K, Rao S, Krey V et al., 2011. RCP 8.5: a scenario of comparatively high green-house gas emissions. Climatic Change, 109,33–57.

Ryan, M. G., 1991. Effects of climate change on plant respiration. Ecological Applications, 1(2), 157-167.

Sano, T., Hirano, T., Liang, N., Hirata, R., Fujinuma, Y., 2010. Carbon dioxide exchange of a larch forest after a typhoon disturbance. For. Ecol. Manage. 260, 2214–2223, doi: 10.1016/j.foreco.2010. 09.026.

Sato, H., Itoh, A., Kohyama, T., 2007. SEIB-DGVM: A new Dynamic Global Vegetation Model using a spatially explicit individual-based approach. Ecol. Modell. 200, 279–307, doi: 10.1016/j.ecolmodel.2006.09.006.

Sato, H., Kobayashi, H., Delbart, N., 2010. Simulation study of the vegetation structure and function in eastern Siberian larch forests using the individual-based vegetation model SEIB-DGVM. For. Ecol. Manage. 259, 301–311, doi: 10.1016/j.foreco.2009.10.019.

Sato, H., & Ise, T., 2012. Effect of plant dynamic processes on African vegetation responses to climate change: Analysis using the spatially explicit individual‐based dynamic global vegetation model (SEIB‐DGVM). Journal of Geophysical

Research: Biogeosciences, 117(G3), 1–18.

Sato, H., Kumagai, T. O., Takahashi, A., Katul, G. G., 2015. Effects of different representations of stomatal conductance response to humidity across the African continent under warmer CO2‐enriched climate conditions. Journal of Geophysical Research: Biogeosciences, 120(5), 979–988.

Sato, T., Yamazaki, H., Yoshida, T., 2017. Extending effect of a wind disturbance: mortality of Abies sachalinensis following a strong typhoon in a natural mixed forest. J. For. Res. 22, 1–7.

Schelhaas, M.J, Nabuurs G.J, Schuck A., 2003. Natural disturbances in the European forest in the 19th and 20th centuries. Glob. Change Biol. 9, 1620–1633.

Sitch, S., Smith, B., Prentice, I.C., et al., 2003. Evaluation of ecosystem dynamics, plant geography and terrestrial carbon cycling in the LPJ dynamic global vegetation model. Glob. Change Biol. 9, 161-185.

Sitch, S, Huntingford C, Gedney N, Levy PE, Lomas M, et al., 2008. Evaluation of the terrestrial carbon cycle, future plant geography and climate-carbon cycle feedbacks using 5 Dynamic Global Vegetation Models (DGVMs). Glob. Change Biol. 14, 2015–2039.

Tanner, E.V.J., Rodriguez-Sanchez, F., Healey, J.R., Holdaway, R.J., Bellingham, P.J., 2014. Long-term hurricane damage effects on tropical forest tree growth and mortality. Ecology 95, 2974–2983.

Ujiie, M., 1984. Studies on the soils derived from volcanic deposits in Tomakomai district [J]. 北海道大學農學部 演習林研究報告 = Research Bulletins of the College Experiment Forests Hokkaido University, 41(1), 149–190.

Usbeck, T., Wohlgemuth, T., Dobbertin, M., Pfister, C., Bürgi, A., Rebetez, M., 2010.

Increasing storm damage to forests in Switzerland from 1858 to 2007. Agric. For. Meteorol. 150, 47–55, doi: 10.1016/j.agrformet.2009.08.010.

Valinger, E, Ottosson Lövenius M, Johansson U, Fridman U, Claeson S, Gustafsson A., 2006. Analys av riskfaktorer after stormen Gudrun. Rapport 8, Skogsstyrelsen, Jönköping 68 pp.

Van Bloem S.J, Murphy P.G, Lugo A.E., 2007. A link between hurricane-induced tree sprouting, high stem density and short canopy in tropical dry forest [J]. Tree Physiology, 27(3), 475–480.

Van Vuuren, D. P., Edmonds, J., Kainuma, M., Riahi, K., Thomson, A., Hibbard, K., ... Masui, T., 2011. The representative concentration pathways: an overview. Climatic Change, 109(1/2), 5.

Van Vuuren DP, Stehfest E, den Elzen MGJ et al. 2011c. RCP2.6: exploring the possibility to keep global mean temperature increase below 2°C. Climatic Change, 109, 95–116

Wang, H. et al., 2004. Net ecosystem CO2 exchange over a larch forest in Hokkaido, Japan. Atmos. Environ. 38, 7021–7032, doi: 10.1016/j.atmosenv.2004.02.071.

Waring, R. H.,1983. Estimating forest growth and efficiency in relation to canopy leaf area. In Advances in Ecological Research (Vol. 13, pp. 327-354). Academic Press.

Watanabe, S., Hajima, T., Sudo, K., et al., 2011. MIROC-ESM 2010: Model description and basic results of CMIP5-20c3m experiments. Geoscientific Model Development, 4, 845–872. https://doi.org/10.5194/gmd-4-845-2011.

Webster, P.J., G.J. Holland, J.A. Curry, H.R.C., 2005. Changes in tropical cyclone number, duration, and intensity in a warming environment. Science 309, 1844–1846, doi: 10.1126/science.1116448.

Xu, X., Hirata, E., Enoki, T., Tokashiki, Y., 2004. Leaf litter decomposition and nutrient dynamics in a subtropical forest after typhoon disturbance. Plant Ecol. 173, 161–170.

Yamanoi, K., Kitamura, K., Mizoguchi, Y., Nakai, Y., 2009. Changes of carbon flux in a broadleaf deciduous forest before and after windthrow disturbance. Proc. AsiaFlux Workshop 2009, pp. 119.

Yamanoi, K., Mizoguchi, Y., Utsugi, H., 2015. Effects of a windthrow disturbance on the carbon balance of a broadleaf deciduous forest in Hokkaido, Japan. Biogeosciences 12(23), 6837. doi:10.5194/bg-12-6837-2015.

Yao, A. W., Chiang, J. M., McEwan, R., Lin, T. C., 2015. The effect of typhoon‐related defoliation on the ecology of gap dynamics in a subtropical rain forest of Taiwan. Journal of Vegetation Science, 26(1), 145–154.

Yazaki, T., Hirano, T., Sano, T., 2016. Biomass accumulation and net primary production during the early stage of secondary succession after a severe forest disturbance in northern Japan. Forests 7, 1–16, doi:10.3390/f7110287.

Yoshida, T., Noguchi, M., 2009. Vulnerability to strong winds for major tree species in a northern Japanese mixed forest: analyses of historical data. Ecological Research, 24(4), 909–919.

Yoshida, T., et al., 2011. Tree mortality in a natural mixed forest affected by stand fragmentation and by a strong typhoon in northern Japan. J. For. Res. 16, 215–222, doi:10.1007/s10310-011-0274-5.

VII. Acknowledgments

First, I would like to express my sincere gratitude to my supervisor, Prof. Kato Tomomichi for his constant encouragement and intellectual guidance during my Ph.D. study. It is my great honor to be a Ph.D. student in the lab of terrestrial ecosystem modeling. Before I came to Japan, I know few knowledges about ecology and modeling. He taught me a lot of basic knowledge. Under his patient teaching, I learned how to use Linux system and how-to programming use Fortran language. He helped me modified every code I wrote, every abstract which I presented on group seminar, domestic and international meeting. He also taught me how to present, how to write paper, how to be a good researcher. When I encountered difficultly in my study, he can give me valuable advice and help me solve the problem. My academic background and research experience have been improved throughout the time studying in his lab. A Chinese proverb said that:' Give a man a fish and you feed him for a day. Teach him how to fish and you feed him for a lifetime.' My supervisor is the man who teach me how to fish and it will help me in my future lifetime.

I would like to offer my special thanks to Dr. Sato who developed the SEIB-DGVM. During learning this model, Dr. Sato patiently teaching me every time when I have some difficulty. In the past three years, he came to our lab several times to communicate and discuss with us and gave me a lot of guidance. I am also grateful to Prof. Hirano and Prof. Sameshima. We are in the same seminar group, they gave me a lot of valuable advice and comments when I presented my study on seminar. Many thanks to Prof. Wang Xiufeng. She gave me and my family a lot of help on our life in Japan. She treats me and my husband as her own child. Her meticulous care made me feel warm in my life abroad. I also appreciated all staffs in Hokkaido university for their kind support.

I would like to take this opportunity to thank all the members of the lab of terrestrial

ecosystem modeling for their help, encourage and support during my Ph.D. study and my life in Japan. I feel very happy and relax with everyone. I also would like to thank the teachers and students in the lab of ecological and environmental physics.

Many thanks to the staff of the Tomakomai Flux Research Site for providing support with the flux-tower data. I am also grateful to the National Institute for Environmental Studies and Tomakomai Flux Research Site for allowing our use of the site. I also thanks to Dr. Tomohiro Hajima (Japan Agency for Marine-Earth Science and Technology) for preparing the MIROC dataset. I also thank the Center for Global Environmental Research, National Institute for Environmental Studies, for providing the phenological photographs of Japanese larch at the Tomakomai site.

My Ph.D. was funded by Japanese Government Scholarship program. I am grateful to the Ministry of Education, Culture, Sports, Science and Technology (MEXT), Japan. With this financial support, I can focus more on my doctoral research.

Finally, I would like to express my deep appreciation to my mom and my husband for their understanding, encouragement, support and always behind me during my study in Japan.

VIII. Appendix

Appendix 1. Processes in the SEIB-DGVM and the approach used to represent each process

	Process	Approach	Source
Physical process	Radiation	Beer's Law within spatially explicit virtual forest	Monteith and Unsworth (1990)
	Evapotranspiration	Penman–Monteith evapotranspiration	
	Soil water process	Analogs of simple bucket model	
Physiology	Photosynthesis	Michaelis-type function	
	Maintenance respiration	The respiration rate is in proportion to the nitrate content of each organ.	Ryan (1991)
	Growth respiration	The respiration rate is based on the chemical composition of each organ.	Poorter (1994)
	Stomatal conductance	A semi-empirical model	Ball et al. (1987) modified by Leuning (1995)
	Phenology	A set of semi-empirical models; parameters were estimated from satellite NDVI data.	Botta et al. (2000) except for BoNS
	Decomposition	Three carbon sources: litter and soil organic carbon with slow and fast decomposition rates	Foley (1995) and Lloyd and Taylor (1994)
Vegetation dynamics	Establishment	Climatically favored PFTs establish as small individuals	
	Mortality	Annual NPP per leaf area, heat stress, bioclimatic limit, and fire	Sitch et al. (2003)
	Fire	Given by an empirical function of soil moisture and aboveground biomass	Kistler et al. (2001)
	Gap formation	Given by an empirical function. This only occurs in tropical rain forest	Huth and Ditzer (2000)

Appendix 2. Formula of light use efficiency and single leaf photosynthetic rate under light saturation

The formula of light use efficiency for C_3 and C_4 PFTs are as follows:

$$\text{lue} = \text{LUE} \times \frac{52 - tmp_{air}}{3.5 + 0.75(52 - tmp_{air})} \times \frac{co2_{cell}}{90 + 0.6 \times co2_{cell}}$$

$$\text{lue} = \text{LUE}$$

where LUE is the potential maximun value, tmp_{air} is the air temperature (℃), $co2_{cell}$ is the intercellular CO2 concentration (μmol mol^{-1}).

The single leaf photosynthetic rate under light saturation is calculated as follows:

$$p_{sat} = \text{PMAX} \times ce_{tmp} \times ce_{co2} \times ce_{water}$$

Where PMAX is the potential maximum of photosynthetic rate, ce_{tmp} is

Modification in SEIB-DGVM

After downloading version 2.82 of SEIB-DGVM (http://seib-dgvm.com/data/seib_code282.zip), the code of SEIB was modified according to Table S1. Latitude and longitude of the Tomakomai site in the file named start_point.f90 was modified. In parameter.txt, the length of the forest stand (Max_loc) and the scenario for establishment (Est_scenario) was also modified. In the main text, the reason why forest stand was expanded from 30 × 30 m to 100 × 100 m was mentioned. There are four establishment scenarios in SEIB. In this study, the Est_scenario 1 was selected, which means only specified woody PFTs can establish. In this scenario, the specified tree can grow by switching (Est_pft_OnOff). Also, all the fire-related code was removed. Then four directories named 1901–1954, 1955–2004, 2005–2016, and 2017–2100 was made and copied the modified model according to Table S1 to these four directories. Table S2 lists the modified corresponding file under each directory.

Appendix 3. Modifications to the simulations of all periods.

File name	Parameter	Original value	Modified value
Parameter.txt	Max_loc	30	100
Parameter.txt	Est_scenario	4	1
Start_point.f90	LAT		42.73
Start_point.f90	LON		141.52
Remove fire component (comment out all fire related code)			

Appendix 4. Modifications to the simulation of period1 (1901-1954)

Directory	Modification
1901–1954	**Parameter.txt**
	simulation_year = 54 !simulation year (y)
	Flag_spinup_write = .true. !flag: make spinup files or not
	Flag_output_write = .true. !flag: make output files or not
	Est_pft_OnOff = .false.,.false.,.false.,.false.,.false,.false.,
	.true.,.false.,.true.,
	.true.,.false.,.false.,.true.,.true.,
	!for Scenario 1: establishment switch

Appendix 5. Modifications to the simulation of period2 (1955–2004)

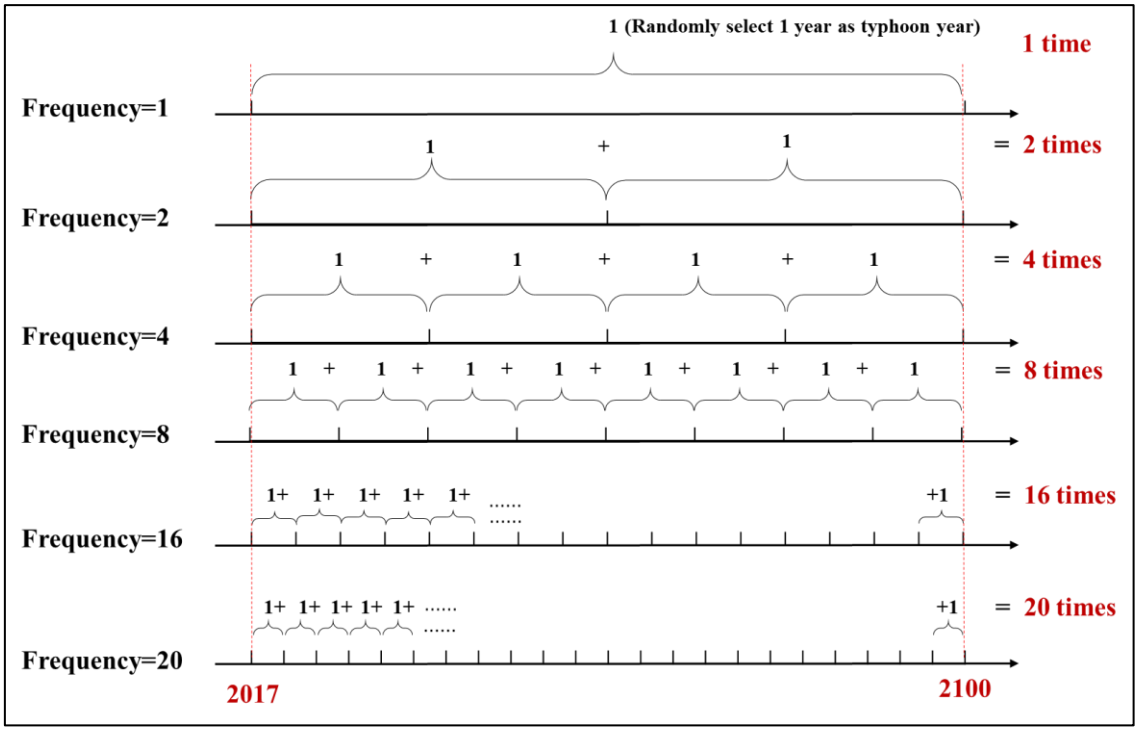
Directory	Modification
1955–2004	**Parameter.txt**
	simulation_year = 50
	Flag_spinup_write = .true.
	Flag_output_write = .true.
	Est_pft_OnOff = .false.,.false.,.false.,.false.,.false,.false.,
	.false.,.false.,.false.,
	.false.,.false.,.false.,.true.,.false.,
	Metabolic.f90
	For BoNS：
	Foliage to dormancy: if (doy = = 306) flag(p) = .true.
	Dormancy to foliage: if (doy = = 112) flag(p) = .true.

Appendix 6. Modifications to the simulation of period3 (2005–2016)

Directory	Modification
2005–2016	**Parameter.txt**
	simulation_year = 12
	Flag_spinup_write = .true.
	Flag_output_write = .true.
	Est_pft_OnOff = .false.,.false.,.false.,.false.,.false,.false.,
	.true.,.false.,.true.,
	.true.,.false.,.false.,.true.,.true.,

Appendix 7. Modifications to the simulation of period4 (2017–2100)

Directory	Modification
2017–2100	**Parameter.txt**
	simulation_year = 84
	Flag_spinup_write = .true.
	Flag_output_write = .true.
	Est_pft_OnOff = .false.,.false.,.false.,.false.,.false,.false.,
	.true.,.false.,.true.,
	.true.,.false.,.false.,.true.,.true.,



Appendix 8. Selection of typhoon year. All the "1" in the figure represent randomly select one year as the typhoon year.

IX. Abbreviations

SEIB-DGVM: Spatial Explicit Individual-Based Dynamic Global Vegetation Model

AGB: Aboveground biomass

GPP: Gross primary production

NPP: Net primary production

NEP: Net ecosystem production

NEE: Net ecosystem exchange

RE: Ecosystem respiration

LAI: Leaf area index

SOM: Soil organic matter

HR: Heterotrophic respiration

PFTs: Plant functional types

DBH: Diameter at breast height

GDD: Growing-degree day

PAR: Photosynthetically active radiation

RCP: Representative Concentration Pathway

CRU: Climate Research Unit

NCEP/NCAR: National Center for Environmental Prediction/National Center for Atmospheric Research

AMeDAS: Automated Meteorological Data Acquisition System

MIROC: Model for Interdisciplinary Research on Climate

AGCM: Atmospheric General Circulation Model

VISIT: Vegetation Integrative Simulator for Trace gases

TMK: Tomakomai Flux Research Site

List of symbols

F: Typhoon frequency

I: Typhoon intensity

$P_{establish}$: establishment probability at vacant patch (m^{-2} $year^{-1}$)

$PMAX$: Maximum photosynthesis rate (μ mol CO_2 $m^{-2}s^{-1}$)

EK: Light attenuation coefficient for vertical direction (dimensionless)

LUE: Control value of light-use efficiency for photosynthesis (mol CO_2 mol $photon^{-1}$)

GDD_{min}: Minimum growth-degree-day sum (5℃ base)

TC_{max}: Maximum coldest-month temperature (℃)

PAR_{min}: Minimum annual average of midday PAR for establishment (μ mol photon m^{-2} s^{-1})

gpp: gross primary production of each tree (g DM day^{-1})

par_{direct}: direct radiation component of par (μ mol photon m^{-2} s^{-1})

$par_{diffuse}$: diffused radiation component of par (μ mol photon m^{-2} s^{-1})

$par_{wood(l,n)}$: midday PAR on crown layer l of individual tree n (μ mol photon m^{-2} s^{-1})